

# Community Detection in Weighted Multilayer Networks with Ambient Noise

Mark He<sup>1</sup>, Dylan Lu<sup>2</sup>, Jason Xu<sup>3</sup>\*, Rose Mary Xavier<sup>2</sup>\*

<sup>1</sup>Statistics & Operations Research, University of North Carolina, Chapel Hill, NC, 27599, USA

<sup>2</sup>School of Nursing, University of North Carolina, Chapel Hill, NC, 27599, USA

<sup>3</sup>Statistical Science, Duke University, Durham, NC, 27708, USA

## Abstract

We introduce a novel class of stochastic blockmodel for multilayer weighted networks that accounts for the presence of a global *ambient* noise that governs between-block interactions. We induce a hierarchy of classifications in weighted multilayer networks by assuming that all but one cluster (block) are governed by unique local signals, while a single block is classified as ambient noise, which behaves identically as interactions across differing blocks. Hierarchical variational inference is employed to jointly detect and typologize block-structures as local signals or global noise. These principles are incorporated into novel community detection algorithm called *Stochastic Block (with) Ambient Noise Model (SBANM)* for multilayer weighted networks. We apply this method to several different domains. We focus on the *Philadelphia Neurodevelopmental Cohort* to discover communities of subjects that form diagnostic categories relating psychopathological symptoms to psychosis.

## 1 Introduction

Relational data have become more common in the advent of sophisticated data gathering mechanisms and more nuanced conceptions of dependency. Statistical network analysis has become a major field of research and is a useful, efficient mode of pattern discovery in complex settings. In many such applications, members within a system are represented as nodes or vertices and their interaction are represented by edges of a graph, including social networks, gene regulatory networks, and ecological webs. Oftentimes, relational information manifest in different modes among the same members. For example, nodes represented by users in a social network such as Twitter can have edges that represent ‘likes’, ‘follows’, and ‘mentions’. In biological networks, many modes of interactions such as gene co-expressions or similarities between biotic assemblages may arise among the same sample of study. These questions are especially pertinent in psychiatric data, where distinct diagnoses are not clearly demarcated, and instead rely on constellations of interacting psychopathologies to properly diagnose certain conditions. In this study, we analyze these multimodal psychopathological symptom data using multilayer network analysis.

General references on statistical modeling of random graphs include the recent works of Newman and Fortunato [26, 46]. While single-graph approaches have been developed decades ago in the social sciences, then in mathematics and physics [7, 12, 27], the literature concerning weighted, dynamic models is much more recent and require more sophisticated methods. Modeling multimodal networks is an emerging field of interest and can be described by Holme et al. [33, 45].

---

\*Joint last author

Alongside the study of networks, the field of *community detection* on networks has grown considerably in recent times, with a host of methodologies from many different fields including computer science, physics, and statistics. Community detection is an approach used to divide a set of nodes in a given relational structure into clusters whose members are strongly connected. Many techniques have been proposed for *unweighted* (binary) graphs including modularity optimization [21, 27], stochastic block models [32, 48, 52, 60], and extraction [38, 61]. Fortunato et al. [26] provide a general overview of different methods.

For community detection in weighted graphs, modularity [27] has also (like binary) received the most emphasis. However, there are numerous limitations to modularity, like asymptotic bias that lead to the discoveries of incorrect community structure [8]. The weighted stochastic blockmodel (SBM) [43] is a model-based approach similar to our proposed method that avoids some of modularity’s pitfalls. Another class of methods as *significance testing* start from a small initializing set of nodes and then gradually incorporate more members until clusters are stable [49, 59]. The advantages to this class of method are in its allowance of overlapping memberships and its accounting for *background* (unclustered) nodes, which are separated but not statistically modeled. Few existing network models actually model noise even though it may be useful in many applications. As such, we develop a model for multilayer weighted graphs that explicitly accounts for:

1. noise present between differing communities, and
2. dependency structure across layers within communities.

This method draws upon the implicit advantages of *noise discovery* from the extraction methods described above, but explicitly models such parts of the network as *ambient noise*. We describe this model as the (Multivariate Gaussian) *Stochastic Block (with) Ambient Noise Model* (SBANM) for the rest of the manuscript.

The contribution of this study is to to develop an algorithm that finds clusters in a multilayer weighted network while simultaneously classifying what *types* of these clusters, namely (local) signal or (global) noise. The proposed method allows joint community discovery of subject clusters in a given clinical sample, while concurrently classifying these clusters. In the primary case study (Section 6), we find clusters of diagnostic subgroups of patients judged by their psychopathology symptoms based on similarity measures, as ground-truths oftentimes do not exist when the psychopathologies are multifaceted and relativistically defined.

## 1.1 Motivation

We posit an example to motivate the natural representation of the proposed model to describe patterns in sociality. Suppose there is a social network where nodes represent members and weights represent social interactions. Members naturally interact in social cliques where rates of communication are roughly similar (i.e. assortative). Across differing communities, however, rates of communication are assumed to be at a baseline noise uniformly spread across the network. Moreover, for members who are *asocial* and do not belong to any community with a unique signal, their interactions are similarly modeled as “noise”, which can be thought of as a *residual* term for connectivity in the linear regression sense. A schematic figure for this model, in comparison to the existing SBM, is presented in Figure 1. We describe three variations of this motivating example in the following subsections.

Psychiatric disorders lack objective measures such as laboratory testing that can confirm or clarify diagnosis. As such, the diagnostic process still rests on clinical assessment

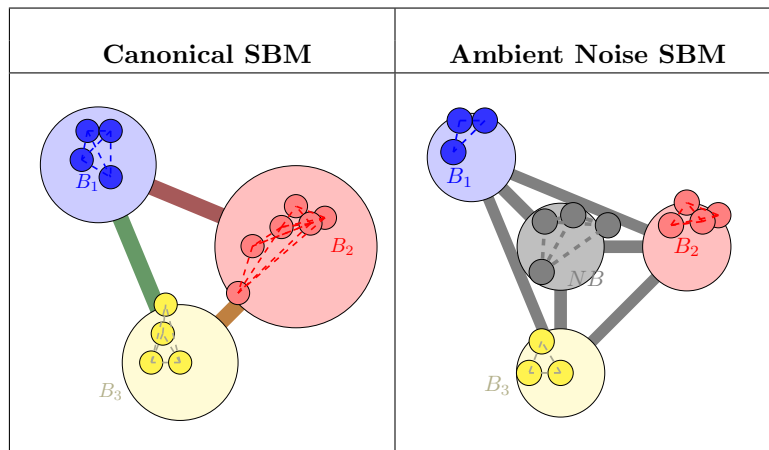


Figure 1: *Illustrative example of the types of relationships between blocks for the canonical SBM (left) and SBANM(right). The dashed lines represent the inter-block connectivity among nodes. The large circles represent distinct communities. The solid thick lines that connect different communities represent the inter-community rates of interaction (transition probabilities if binary). In the canonical case (left), the inter-block transitions are all distinct, as denoted by its colors. For the SBANM case (right), the inter-block parameters are all the same (represented by gray); AN governs the connectivities between blocks and the intra-block connectivity within the block NB.*

and is built on codified symptom domains such as positive, negative and cognitive symptoms in the case of psychosis [35]. However, the flagship criterion that defines the diagnosis of many psychotic disorders such as schizophrenia is the presence of positive symptoms. This traditional categorical diagnostic system stipulated in the Diagnostic and Statistical Manual [6] has clinical utility but leads to an excess of diagnostic comorbidities and heterogeneities in the clinical presentation of illnesses [20, 37, 57].

Though the clinical diagnostic criteria identifies patients that need treatment, it does not provide an understanding of the neurodevelopmental trajectories or mechanisms of illness, which is necessary for developing effective treatments. Data-driven approaches for clinical problems have become more useful in light of these challenges. We approach this problem quantitatively by applying SBANM to the weighted multilayer graphs that represent symptom data. Psychiatric illnesses have multiple causalities and symptoms. Schizophrenia, for example, is a “chronic, psychotic, neuropsychiatric, genetically complex, and clinically heterogenous” brain disorder that affects millions worldwide. One issue of clinical importance is the difficulty in identifying individuals who are at risk for developing psychosis.

In most existing research, nodes represent known entities and edges are known quantities between individuals. For example, in analyses of Twitter/Facebook networks [51], nodes and edges are observed. This assumption can not be typically applied to psychiatric network models to identifyin–g communities of individuals with similar psychopathologies. In the clinical setting, either

1. connections must be estimated from clinical, biological, or psychosocial data, or
2. the goal is early identification and diagnosis from the unknown categories using estimated connections to establish new ground truths for clinical settings.

With an increase in availability of multimodal data across populations of clinical subjects,

multilayer community detection is a natural tool for the analysis and classification of psychiatric illnesses with multifaceted characteristics.

While the application to assess diagnostic categories for psychosis will be the primary focus of the proposed methodology, it is useful to find latent structure in other types networks. In addition to the PNC data, we also demonstrate the method on (1) US congressional voting data and (2) human mobility (bikeshare) data. We use SBANM to find latent patterns in longitudinal US congressional co-voting data to analyze the static as well as dynamic patterns in co-voting amongst US congressional districts, historically a fruitful domain of network analysis [19]. We also find clusters in longitudinal aggregations of bikeshare networks, whose stations are represented by nodes. Analysis of zones amongst urban mobility services is elucidating for discovering latent patterns within human geography and demographic trends [17, 18, 28]. Description of the data can be found in Section 2 and details on the analyses are found in Section 5.

## 1.2 Background and Contributions

Though much work has been done on differing types of estimation for stochastic block-models assuming assortative structure as well as distinct inter-block characteristics, there has not been much study focused on estimating the *noise* inherent within stochastic block-models, much less for multilayer weighted graphs. The primary motivation for developing a multilayer blockmodel with noise is to capture the structure of weighted networks with a notion of a global *residual* (as in regression analysis). The notion of noise has not been explored at length in the study of networks, especially in SBMs. Extraction-based methods mentioned in the prior section incorporate background nodes to signify lack of community membership [49, 59]. However, these methods are not model-based and do not attribute any parametric descriptions (only a lack thereof) to these background nodes. Some recent work discuss noise in network models that are oftentimes associated with global (i.e. entire-network) uncertainty that is uniformly added to all edges [10, 47]. However, few studies have studied *structural noise* that affects, or constitutes, entire communities.

The canonical example of a globally noisy network is the Erdos-Renyi model where every connection in the network is governed by a single probability. Allman et al. prescribe a simple model known as the affiliation model on weighted networks [4] used to describe a ‘noisy homogeneous network’. In the affiliation model, a single *global* parameter that dictates the connectivity between all nodes in *any* community, and another global parameter that controls for the connectivity for all members in differing communities.

The SBM is a seminal generative (as if one were to generate a simulated network from a given set of parameters) model for random graphs. Beyond theory, the SBM has also found empirical functionality in community detection. Many approaches from multiple perspectives [36, 52] provide ways of characterizing and estimating the model. First proposed to describe binary networks [30, 48], the model has been extended to weighted [43]) and multilayer settings [44, 50, 55]. Matias et al. [44] propose a dynamic SBM over time series of weighted and binary networks. Clusters across all time points have the same inter-block parameters, but varying between-block interactions. Most studies do not account for correlations among blocks across layers.

The weighted SBM and the affiliation model are both cases of the *mixture models for random graphs* described by Allman et al. [4, 5]. This general class of network models accounts for assortativity (the tendency for nodes who connect to each other at similar

rates or intensities to cluster together) as well as sparsity (when there are much fewer edges than nodes). For many typical graph-data representations, “sparsity” is represented by zeroes to signify absence of edges. However, for many weighted networks, zeroes may not mean absence, particularly if the weights assume negative values. This is often the case if weights are normalized (i.e. Fisher transformation). As such, the notion of ‘sparsity’ varies in existing approaches and may be better represented by a baseline *ambient noise* in weighted networks.

We propose a model that possesses qualities of both the affiliation model as well as the weighted stochastic blockmodel. The weighted affiliation model described in the previous section fixes connectivities globally across the whole network may be descriptive of the ambient, baseline effects of noise, but where clusters emerge within the network that yield unique local effects. Like the *local* stochastic block model, the postulated model is *locally unique* with parameter  $\boldsymbol{\theta}_q$  (multivariate vector with  $K$  dimensions) for all edges between nodes within each block  $q, l$ , but also has noise parameter  $\boldsymbol{\theta}_{\text{Noise}}$  that, like the affiliation model, globally describes all interactions between nodes in differing blocks:

$$\boldsymbol{\theta}_{ql}^* = \begin{cases} \boldsymbol{\theta}_q & \text{if } q = l \\ \boldsymbol{\theta}_{\text{Noise}} & \text{if } q \neq l \end{cases}. \quad (1)$$

This model lends more realism for many empirical scenarios described in the above sections. The notion of a reference or *null* group is useful and oftentimes necessary for clinical applications. In samples with *normal control* groups, such a network formulation is oftentimes needed for testing and validation: in regions-of-interest (ROI) analysis in brain networks for example, the cerebellum is used as a reference region. The method also best describes the commnality in *out-of-clique* and *baseline* modes of communication in the motivating example described in the first paragraph of Section 1.1.

Another motivation for this model is its parsimony compared to the canonical SBM. Existing clustering models on multilayer networks, even when accounting for communities that persist across layers [41], still tend toward overparameterization. Mixed-membership blockmodels are related to noise in that it attributes some level of uncertainty in exact membership designations, like Airoldi et al. [2], but doubly complicate the model parameter landscape with overlapping block combinations. Our model seeks to simplify the notion of ambiguous memberships by subsuming their characteristics into an umbrella ambient noise term that describes the ambiguities in block memberships in the common interstitial noise term for all interactions amongst members in differing blocks. SBMs in both binary and weighted settings are identifiable across both static (single network) and multilayer settings [44]. Because both the affiliation model and the multilayer SBM are proven to be identifiable by prior work [4, 44], we posit that **SBANM** is also identifiable. A brief argument is given in Appendix E, but more rigorous justification remains as future work.

In the rest of the paper, we motivate with the data in the main case study in Section 2. We then describe the model and its method of (variational) inference in Section 3, and the specific mechanics and steps of the estimation algorithm in Section 4. Model performance is compared with other existing methods in Section 5.1.5. Following the simulation analyses, we apply the method to political and human mobility datasets in Sections 5.2 and 5.3. In Section 6, we demonstrate the focal case study of psychopathology symptom data.

## 2 Data

The sample for the primary case study was obtained from the PNC cohort which includes data from 9498 youth from the greater Philadelphia area, aged 8-21 years who received a detailed neuropsychiatric evaluation [13, 14]. The PNC has a well-represented sample with mostly European American ancestry but a substantial portion of African Americans. Roughly 21% met psychosis spectrum criteria, 4% reported threshold psychosis symptoms, 12% reported subthreshold positive symptoms, 2% exhibited subthreshold negative symptoms ([15]). We separately analyze the two age cohorts *youth* (with sample size 5136) and *early adult* (sample size 1863) in the following sections.

Response networks are constructed using a function that gauges similarity as well as positivity or negativity of responses. This distance function is similar to Hamming distance, but is between -1 and 1 and takes into account the direction of *positive* or *negative* agreement. In a single graph-layer  $\mathbf{X}^k$ , a weight  $X_{ij}^k$  between two nodes is derived from indicators  $h_{ij,u}^k$  across  $U$  questions (indexed by  $u$ ) pertaining to a given set of conditions.

$$h_{ij,u}^k = \begin{cases} 1 & \text{if } i, j \text{ both answer "yes"} \\ -1 & \text{if } i, j \text{ both answer "no"} \\ 0 & \text{otherwise} \end{cases}$$

These values  $h_{ij,u}$  are then summed and divided by the total number of questions  $U$ :

$$r_{ij}^k = \frac{\sum_{u=1,\dots,U} h_{ij,u}^k}{U}.$$

The weight  $r_{ij}^k$  is 1 if two subjects both answer yes to everything and -1 if they answer no to everything. The weight  $r_{ij}^k$  is then transformed using a Fisher transformation to produce a value that approximates an observation in a normal distribution, in layer  $k$ :  $X_{ij}^k = \text{Fisher}(r_{ij}^k)$ .  $X_{ij}^k$  is assumed to be generated from clusters of nodes that follow blockwise multivariate normal distributions. More details are listed in Section 3.1. We use three general categories of disorders to represent each layer:

1. Anxiety ( $\mathbf{X}^x$ ): 44 questions (generalized, social, separation anxiety, etc.)
2. Behavior ( $\mathbf{X}^y$ ): 22 questions (ADHD, OCD, CDD)
3. Mood ( $\mathbf{X}^z$ ): 10 questions (depression and mania)

Each  $h_{ij,u}^k$  between two subjects  $u, v$  is -1 if both answer no, 1 if both yes, otherwise 0. These values are then summed, divided by the number of survey questions, then Fisher-transformed to produce the weighted edge in graph  $\mathbf{X}^k$  in layer  $k$ . In these following sections these categories will simply be referred to as “anxiety”, “behavior”, and “mood”.

The focus of the study is on the PNC data. However, we also show the model’s generality by applying the method to political and human mobility data. We use congressional voting records from *Voteview* to uncover patterns in US congressional voting patterns that may yield more nuanced political groups than party labels (i.e. Democrat, Republican) over time. We use a similar pre-processing step as done for the PNC data to assign measures for co-voting similarities between seats in the US House of Representatives during the 100th, and 115th sessions. Voting similarities between representatives in Congress are represented as weighted edges between nodes (representing members). Each layer corresponds to a different congressional session. We apply the proposed model to data from

the *Divvy* bikeshare system in Chicago called to show the ways that demarcating zones of bikeshare trips change across different years. Trip data for Divvy are publicly available on their respective websites [24]. More detailed descriptions of the procurement and pre-processing of both datasets can be found in the later Sections 5.2 and 5.3 .

### 3 Model and Inference

The proposed model combines characteristics from the weighted *affiliation model* with the weighted SBM. SBANM supposes that networks across  $K$  layers have the same block structure, while transition parameters between blocks are fixed at the same global, *ambient*, level. This model presumes block structures whose edges are correlated across layers. This formulation of blockmodel allows detection of common latent characteristics across layers, as well as differential sub-characteristics within blocks (represented by multivariate normal distributions) which are generally similar (as to be drawn from the same distribution). Whether the assumption of correlated multilayer blockstructures with ambient noise inherently fits the data-generation mechanism, the method of clustering glean information from the multilayer network reductively and sufficiently.

#### 3.1 Notation and Terminology

For **weighted** graphs spanning  $K$  layers and the same (registered)  $n$  nodes indexed by the set  $[n] = \{1, 2, \dots, n\}$ , let  $\mathbf{X}$  represent the collection of multilayer weighted graphs with  $K$  layers:  $\mathbf{X} = \{\mathbf{X}^1, \mathbf{X}^2, \dots, \mathbf{X}^K\}$ . We let  $\mathbf{X}_{ij} = (X_{ij}^1, X_{ij}^2, \dots, X_{ij}^K)$  represent the multidimensional vector of edge-weight  $(i, j)$  across all layers  $k = 1, 2, \dots, K$ . For a community  $B_q \subset [n]$  representing the nodes that are contained in block  $q$  in a weighted multilayer network  $\mathbf{X}$ , we let  $\mathbf{X}_q$  represent the set of all edges contained in block  $q$  across all  $K$  layers:

$$\mathbf{X}_q = \{\mathbf{X}_{ij}\}_{i,j \in B_q}. \quad (2)$$

Moreover, the set of edges across different blocks  $q, l$  where  $q \neq l$  (i.e. interstitial noise), are expressed as:

$$\mathbf{X}_{IN} = \{\mathbf{X}_{ij}\}_{i \in B_q, j \in B_l}. \quad (3)$$

Finally, we fix **one** block indexed as  $NB$  as a “noise block” such that all weights within the block have mean and variance parameters  $\boldsymbol{\mu}_{NB}$  and  $\boldsymbol{\Sigma}_{NB}$ . This block represents a null region that is devoid of unique signal, but is distributionally governed by the same characteristics as the interstitial relationships between different blocks. We let  $\mathbf{X}_{NB}$  represent the set of edges among members in the “noise block”:  $\mathbf{X}_{NB} = \{\mathbf{X}_{ij}\}_{i,j \in NB}$ . In the following subsection we describe the data as introduced in the prior section in the context of the notation. In Section 3.2 we describe the key assumption classifying this notion of noise.

##### 3.1.1 Mapping Notation to Data

We represent each of the described data-forms in the aforementioned Section 2 with multilayer networks. Multilayer networks can represent multiple modes of relationships, or *time-window* (longitudinal) graphs, as well as *difference graphs*, which describe differential settings or test conditions of an interacting system. [33, 45]. The applications outlined in Section 5 both are examples of longitudinal graphs, while the primary case study for

PNC data constitute multimodal networks. In each application, we write the weighted graph-system  $\mathbf{X}$  with  $K$  layers and define the index set  $[n]$  as the set (of cardinality  $n$ ) of all nodes. Every layer has  $n$  nodes and each weight  $\mathbf{X}_{ij}$  between nodes  $i, j$  is written as a  $K$ -dimensional vector, and each layer-specific (at  $k$ ) weight is written as  $\mathbf{X}_{ij}^k$ .

For the PNC data,  $\mathbf{X}$  represents the whole set of anxiety, behavior, and mood psychopathology symptom networks across a given set of subjects. There are three layers and each  $k$  ( $x, y$ , and  $z$ ) represents one of the psychometric evaluation networks representing each disorder. The sample size  $n$  in this context represents the 5136 subjects between the ages of 11 to 17 (*youth*) and 1863 between the ages of 18 to 21 (*early adult*). Each node represents a subject, and each weighted edge the transformed similarity ratio between two subjects for anxiety, behavior, and mood disorders.

In the voteview data, each layer represents interactions among each congressional session.  $(\mathbf{X}, \mathbf{Y})$  represents the 100th and 115th sessions of congress, respectively.  $n$  represents the number of congressional seats that are common to all three sessions (new or relabeled seats that were added since the first session are not included) Only two layers are used for this application of SBANM to the Divvy data, and  $(\mathbf{X}, \mathbf{Y})$  in this case represents the normalized, aggregated trips between 2014-2016 and 2016-2018 respectively. The sample size  $n = 547$  describes the total number of stations and each edge weight represents aggregate trips between stations.

### 3.2 Multilayer Gaussian Weighted Graphs

In this section we define Multilayer Gaussian Weighted Graphs and their ambient noise characteristics.

**Definition 1.** (*Correlated Gaussian Blocks between Layers*) We denote block indices  $q = 1, \dots, Q$  with corresponding communities  $B_1, B_2, \dots, B_Q$ , where for each  $q$ ,  $B_q$  are disjoint and such that the union of the total communities  $\bigcup_{q=1, \dots, Q} B_q = [n]$ . Each weighted edge between any node housed within each block  $B_q$  form a multivariate normal distribution with mean  $\boldsymbol{\mu}_q = (\mu_{q,1}, \dots, \mu_{q,K})$  which is a  $K$  dimensional vector, and covariance matrix  $\Sigma_q$  which is a  $K \times K$  matrix. In  $\Sigma_q$  with diagonal as the variance and off-diagonal entries as covariances between layers:

$$\Sigma_q = \begin{pmatrix} \sigma_{q,1}^2 & \rho_q \sigma_{q,1} \sigma_{q,2} \dots & \rho_q \sigma_{q,1} \sigma_{q,K} \\ \rho_q \sigma_{q,2} \sigma_{q,1} & \sigma_{q,2}^2 \dots & \rho_q \sigma_{q,2} \sigma_{q,K} \\ \dots & \dots & \dots \\ \rho_q \sigma_{q,K} \sigma_{q,1} & \dots & \sigma_{q,K}^2 \end{pmatrix}.$$

For nodes  $i, j$  in a  $K$ -layer multilayer weighted network, where, if  $i$  belongs to block  $q$  and  $j$  belongs to block  $l$ , the distribution of edges follow

$$\mathbf{X}_{ij} | \{i \in B_q, j \in B_q\} \sim N_K(\boldsymbol{\mu}_q, \Sigma_q).$$

We assume that the *Noise Block* as has the same characteristics as the *Interstitial Noise*. The mean and variance of *NB* and *IN* are both drawn from the same distribution *AN* (*Ambient Noise*).

**Assumption 1.** *AN is a global noise term such that the distributions of IN and NB are identical:*

$$\begin{aligned} \mathbf{X}_{IN} &\stackrel{d}{=} \mathbf{X}_{NB} \\ &\sim N_K(\boldsymbol{\mu}_{AN}, \Sigma_{AN}). \end{aligned}$$



Because  $NB$  and  $IN$  both represent “baseline” levels of connectivity for the network, we assume that they both have equivalent characteristics as  $AN$ . Members of each block  $B_q$  interact with other members in the same block with edges which follow rates that follow multivariate  $\boldsymbol{\mu}_q$  with variance  $\boldsymbol{\Sigma}_q$ , but interact with members in differing groups  $l; l \neq q$  at baseline rates  $\boldsymbol{\mu}_{IN}$  with variance  $\boldsymbol{\Sigma}_{IN}$ , i.e. background interactions.

**Definition 2.** (*Ambient Noise*) Edges between members from differing blocks, as well as edges between members in the noise block  $NB$ , are characterized by the same distribution  $(\boldsymbol{\mu}_{AN}, \boldsymbol{\Sigma}_{AN})$ :  $\boldsymbol{\mu}_{AN} = (\mu_{AN,1}, \dots, \mu_{AN,K})$  and  $\boldsymbol{\Sigma}_{AN}$  which is a diagonal matrix with diagonal  $(\sigma_{AN,1}^2, \dots, \sigma_{AN,K}^2)$  and with zeroes as off-diagonal entries. For blocks  $q \neq l$ :

$$\mathbf{X}_{ij} | \{i \in B_q, j \in B_l\} \sim N_K(\boldsymbol{\mu}_{AN}, \boldsymbol{\Sigma}_{AN}).$$

For a community  $B_q \subset [n]$  representing the nodes that are contained in block  $q$  in a weighted multilayer network  $\mathbf{X}$ , we let  $\mathbf{X}_q$  represent the set of all edges contained in block  $B_q$  across all  $K$  layers as defined in Equation (2). Conversely, the set of edges across differing  $B_q, B_l$  (i.e. interstitial noise), are defined as in Equation (3).

**Definition 3.** (*Stochastic Block (with) Ambient Noise Model*) A multilayer weighted network  $\mathbf{X}$  with  $n$  nodes across  $K$  layers is a *Multivariate Gaussian Weighted Stochastic Block (with) Ambient Noise Model* (SBANM) with  $Q$  blocks if these following conditions are satisfied:

1. Edges between nodes with memberships in the same blocks follow the assumptions in Definition 1 i.e. for each edge  $i, j$  in block  $B_q$ , the conditional distribution of the edges follows  $N_K(\boldsymbol{\mu}_q, \boldsymbol{\Sigma}_q)$ .
2. Ambient noise  $AN$  with  $N_K(\boldsymbol{\mu}_{AN}, \boldsymbol{\Sigma}_{AN})$  that governs both interstitial relationships between nodes  $IN$  in differing signal blocks  $B_q$ , as well as noise block  $NB$ :
  - (a) Edges between nodes with memberships in differing blocks follow: for each edge  $i \in B_q$  and  $j \in B_l$ , the conditional distribution of the edge-weights follow a  $N_K(\boldsymbol{\mu}_{AN}, \boldsymbol{\Sigma}_{AN})$  distribution.
  - (b) **One** block  $NB$  contains members whose edges are generated from a  $K$ -dimensional multivariate normal distribution  $N_K(\boldsymbol{\mu}_{AN}, \boldsymbol{\Sigma}_{AN})$ .

### 3.3 Variational Inference

We use variational inference (VI) to estimate the memberships and the parameters of the proposed model. Variational Expectation Maximization (VEM) has historically been used for estimating SBM memberships as well as their parameters [34]. Variational inference is an approach to approximate a conditional density of latent variables using observed information by solving this problem with optimization [9]. Instead of using the full likelihood, a simpler surrogate is chosen. These differences (in terms of Kullback-Liebler (KL) Divergence) between the surrogates and the desired variables are then refined and minimized to the smallest possible values. Oftentimes, and especially in the context of community detection problems, mean-field approximations serve as simpler, independent, surrogates of latent approximands.

Variational EM (VEM) has been demonstrably efficient when other approaches have been computationally intractable [43]. MCMC-based attempts to estimate memberships, for example, are prohibitively slow and only allow estimation up to 200 nodes [48]. VEM

has been the state-of-the-art approach for most studies in SBM estimation. Daudin et al. was introduced using VEM for binary-graph SBMs ([23]. Mariadassou et al. used a similar method for clustering on a single weighted graph [43], while Matias et al. also did so for multilayer networks [44]. Our estimation algorithm is also rooted in variational EM, but we augment the procedure with *signal* and *noise* typologizing different blocks.

Hierarchical Variational Inference (HVI) provides a natural framework for the two-layered latent structure for multilayer networks. For multilayered networks, an interpretable tiered hierarchy of community structure arises from the connections between networks. Though it enables efficient inference, “typical” mean-field variational inference is limited by its assumption of strong factorization and does not capture posterior dependencies between latent variables arising amongst multilayered networks. A natural hierarchy is induced in SBANM by the assumption that all but one block are under the umbrella of *signal*, while a single block is classified as noise. HVI augments variational approximations with priors on its parameters. This assumption allows joint clustering of blocks as the *basal* structure and the blocks’ signal-noise differentiation as the *superstructure*.

We use a similar approach to that originally used in Daudin et al. [23]. The main difference from those approaches is that we are dealing with joint approximate conditional distributions instead of a univariate  $\mathbf{Z}$  (representing block memberships).

$$R_{\mathbf{X}}(\mathbf{Z}, \mathbf{C}) \approx \prod_{i,q} \left( m(\mathbf{Z}_i, \boldsymbol{\tau}_i) \times \text{Bern}(C_q, P_q) \right) \quad (4)$$

In Eq. (4)  $R(\cdot)$  represents the joint variational distribution of the memberships  $\mathbf{Z}, \mathbf{C}$ , or the posterior distribution of the mean field distributions. We do not know the exact joint distribution, but we can use the mean field approximation to obtain a factorized estimate for its marginals and write the approximate composition of marginals using “ $\times$ .” Here  $m(\cdot)$  represents the multinomial distribution,  $\boldsymbol{\tau}$  represents the vector of probabilities of length  $Q$  that approximates  $Q$ -dimensional membership vectors  $\mathbf{Z}_i$  [43]. The variational approximations of membership matrix  $\mathbf{Z}$  is a  $n \times Q$ -dimensional matrix  $\boldsymbol{\tau}$ . The variational approximation of the indicator  $C_q$  at block  $q$  is the probability  $P_q$ , which typologizes and hence “sits at a higher tier” in the hierarchy than  $\boldsymbol{\tau}$ . Under variational distribution  $R$ , each member  $i$  of a block  $B_q$  adheres to multinomial distribution with parameter  $\tau_{iq} = \mathbb{E}[\mathbf{Z}_{iq}]$ ,

We use an indicator random variable to determine if a block  $q$  is signal or noise  $NB$ .  $\mathbf{C}$  represents the “membership of memberships” where each block is either a member of *signal* or *noise* blocks. Since there are only two designations,  $\mathbf{C}$  is a vector of length  $Q$  whose values  $C_Q$  are 0 or 1.  $P_q$  is the probability of  $C_Q$  akin to  $\tau_{iq}$ , and form an Bernoulli distribution with parameter  $P_q$  marginally. For each  $q$ ,  $P_q$  is ambient noise with prior probability  $\Psi$ . One can think of  $\Psi$  as the membership-of-memberships probability analogous to  $\boldsymbol{\alpha}$  for  $\boldsymbol{\tau}$ . A derivation for  $\Psi$  is given in Appendix C.5.

**Definition 4.** Let  $\Psi$  be the parameter for the probability of any node in the multilayer graph system to belong to a noise block.

$$\Psi := (Q - 1)/Q \quad (5)$$

*i.e.* the probability of selecting a node from  $NB$  when a single node is selected from the total collection of nodes. In this case of the multivariate weighted SBM, the model is constrained by the presence of a single block that espouses the distributional characteristics as the interstitial noise.

Ranganath et al. [53] defined the hierarchical variational model as a two-level distribution. The distribution “marginalizes out” the mean-field parameters in the mean-field distribution  $R_{\mathbf{X}}(\mathbf{Z}, \mathbf{C})$ . The hierarchical distribution  $R_{\text{hv}}(\mathbf{Z})$  is then written as

$$R_{\text{hv}}(\mathbf{Z}) = \int R_{\mathbf{X}}(\mathbf{Z}, \mathbf{C}) d\mathbf{C}.$$

Following the methods of estimation proposed in prior work on SBM estimation [23, 43, 51], we posit that  $R_{\mathbf{X}}(\mathbf{Z}, \boldsymbol{\tau})$  represents the multinomial variational distribution wherein each  $\tau_{iq}$  approximates the membership vector itself. We posit latent element  $\mathbf{C}$  that governs whether the block itself is *signal* or *noise*. As such, the integrated  $R_{\text{hv}}(\mathbf{Z})$  represents the distribution in prior work that is not subject to the signal or noise categorizations.

Prior work that use VEM for SBM estimation focuses on Evidence Lower Bound (ELBO) maximization [23, 43, 50, 51]. We define the ELBO below.

**Definition 5.** (*Evidence Lower Bound (ELBO)*) Given observed data  $\mathbf{X}$  with unknown latent membership variables  $\mathbf{Z}$ , the evidence lower bound (ELBO)  $\mathcal{L}$  is the approximately optimal likelihood that minimizes the KL Divergence between the approximate distribution  $R(\mathbf{Z}, \mathbf{C})$  and the posterior frequency  $f(\mathbf{Z}, \mathbf{C}|\mathbf{X})$ . It is expressed as follows:

$$\mathcal{L} = \mathbb{E}_{R_{\text{hv}}(\mathbf{Z})} [\log f(\mathbf{Z}, \mathbf{X}) - \log R_{\text{hv}}(\mathbf{Z})]$$

Alternatively, the ELBO can be rewritten as the sum of the expected frequency and the entropy  $\mathcal{H}$  of variational variable  $\mathbf{Z}$ :

$$\mathcal{L} = \mathbb{E}_{R_{\text{hv}}(\mathbf{Z})} [\log f(\mathbf{Z}, \mathbf{X})] + \mathcal{H}_{\text{hv}}(R(\mathbf{Z})).$$

A better bound than the ELBO is derived by introducing the marginal posterior approximate distribution  $S$  of  $\mathbf{C}$  and analyzing  $\mathbf{KL}(R, S)$ .  $S(\mathbf{C}|\mathbf{Z})$  represents the variational approximation model for the posterior distribution  $R$  given the memberships  $\mathbf{Z}, \mathbf{C}$ . This bound is sharper than the ELBO because it takes into account the entropy of  $R$ . We reproduce a proposition from prior work as follows; a proof of this proposition is given in Appendix A.1 [53].

**Proposition 1.** For observed data  $\mathbf{X}$  and membership matrix  $\mathbf{Z}$ , if the membership matrix  $\mathbf{Z}$  are structured hierarchically, with overarching layer  $\mathbf{C}$  which partition the membership variables  $\mathbf{Z}$  into groups, and with joint distribution  $R(\mathbf{Z}, \mathbf{C})$ , then the Hierarchical ELBO provides a better approximation of the true log-likelihood: i.e. a lower evidence lower bound.

### 3.4 Parameter Estimation

In a graph  $\mathbf{X}$  with  $K$  graph-layers  $\{\mathbf{X}^1, \dots, \mathbf{X}^K\}$  where each edge between nodes  $i, j$  of each graph, the conditional density given membership estimates is written as

$$\begin{aligned} & \log(f(\mathbf{X}|\mathbf{Z})) \\ &= \sum_{q:q \neq NB} \left( \sum_i \sum_j \tau_{iq} \tau_{jq} \left( \frac{1}{2} (\mathbf{X}_{ij} - \boldsymbol{\mu}_q)^T \boldsymbol{\Sigma}_q^{-1} (\mathbf{X}_{ij} - \boldsymbol{\mu}_q) - (2\pi)^{K/2} (\log |\boldsymbol{\Sigma}_q|)^{1/2} \right) \right. \\ & \quad \left. + \mathbf{1}(q = NB) \sum_{i,j} \tau_{iq} \tau_{jl} \left( \frac{1}{2} (\mathbf{X}_{ij} - \boldsymbol{\mu}_{AN})^T \boldsymbol{\Sigma}_{AN}^{-1} (\mathbf{X}_{ij} - \boldsymbol{\mu}_{AN}) - (2\pi)^{K/2} (\log |\boldsymbol{\Sigma}_{AN}|)^{1/2} \right) \right) \\ & \quad + \sum_{q:l:q \neq l} \sum_{i,j} \tau_{iq} \tau_{jl} \left( \frac{1}{2} (\mathbf{X}_{ij} - \boldsymbol{\mu}_{AN})^T \boldsymbol{\Sigma}_{AN}^{-1} (\mathbf{X}_{ij} - \boldsymbol{\mu}_{AN}) - (2\pi)^{K/2} (\log |\boldsymbol{\Sigma}_{AN}|)^{1/2} \right). \quad (6) \end{aligned}$$

Each  $\mathbf{X}_{ij} = (X_{ij}^1, \dots, X_{ij}^K)$ , The log likelihood portion of the ELBO  $\log(f(\mathbf{X}|\mathbf{Z}))$  written above in Equation (6) is comprised of three parts: unique signals for every  $q$  (top), the noise block  $NB$  (middle), and the interstitial noise  $IN$  (bottom).  $AN$  is the global *ambient noise* whose parameters govern the *interstitial noise* as well as *noise block* as in Assumption 1. The probabilities of the blocks  $B_q$  “being signal” are demarcated by  $P_q$  and “being noise” by  $1 - P_q$ . Given that we know the variational variables  $\boldsymbol{\tau}, \mathbf{C}$ , the expected likelihood is

$$\begin{aligned} \mathbb{E}_{R_{\mathbf{X}}}[\log(f(\mathbf{X}|\mathbf{Z}))] &= \sum_{q:1 \leq q \leq Q} \mathbb{P}(B_q \text{ is not } NB) \cdot \tau_{iq} \tau_{jl} f(\mathbf{X}|C_q = 1) \\ &+ \mathbb{P}(B_q \text{ is } NB) \cdot \sum_{i,j:i \neq j} \tau_{iq} \tau_{jl} f(\mathbf{X}|C_q = 0) + \sum_{q,l:l \neq q} \sum_{i,j:i \neq j} \tau_{iq} \tau_{jl} f(\mathbf{X}|C_q = 0). \end{aligned}$$

The  $\mathbb{E}_{R(\mathbf{Z}, \mathbf{C})}[\log f(\mathbf{Z})]$  term restores to the same form as earlier iterations of SBMs [23, 43]:

$$\mathbb{E}_{R(\mathbf{Z}, \mathbf{C})}[\log f(\mathbf{Z})] = \sum_{i,q} \tau_{iq} \log \alpha_q. \quad (7)$$

Since the expected log frequency of the membership vectors  $\mathbf{Z}$  reduces to that in canonical SBMs. Details of this identity is found in Appendix A.2. The joint density is written as:

$$\mathbb{E}_{R(\mathbf{Z}, \mathbf{C})}[\log f(\mathbf{X}, \mathbf{Z})] = \mathbb{E}_{R(\mathbf{Z}, \mathbf{C})}[\log f(\mathbf{X}|\mathbf{Z})] + \sum_{i,q} \tau_{iq} \log \alpha_q. \quad (8)$$

The expression is written in full in Appendix B.1.

Model parameters can be partitioned into  $\Theta_{\text{Signal}}$  and  $\Theta_{\text{Noise}}$  in addition to global parameters  $\boldsymbol{\alpha}, \Psi$ . We write the entire set of model parameters as

$$\Theta = \{\boldsymbol{\alpha}, \Psi, \Theta_{\text{Noise}}, \Theta_{\text{Signal}}\}. \quad (9)$$

As in prior work [23, 43], the variables  $\alpha_q$  represent the membership probabilities of  $Z_{iq}$  and sum to 1:

$$\alpha_q = \mathbb{P}(i \in B_q) = \mathbb{P}(Z_{iq} = 1). \quad (10)$$

$\Theta_{\text{Signal}}$  represents the model parameters that are unique to each block  $B_q$  (not including  $NB$ ), and also there is one fixed label  $q_{(NB)}$  that indexes the noise block  $NB$ .  $\Theta_{\text{Noise}}$  represents the noise parameters that govern both interstitial noise  $IN$  and noise block  $NB$ :

$$\Theta_{\text{Signal}} = \{\boldsymbol{\mu}_q, \boldsymbol{\Sigma}_q\}_{q:1 \leq q \leq Q}; \quad \Theta_{\text{Noise}} = \{\boldsymbol{\mu}_{AN}, \boldsymbol{\Sigma}_{AN}\}.$$

For  $NB$ , moreover, each correlation between layers is set at zero.

### 3.5 Decomposition of the Hierarchical ELBO

The hierarchical ELBO  $\mathcal{L}'$ , which was defined in Definition 5 can be decomposed as

$$\mathcal{L}' = \mathbb{E}_{R(\mathbf{Z}, \mathbf{C})} \log f(\mathbf{X}, \mathbf{Z}) + \mathbb{E}_{R(\mathbf{Z}, \mathbf{C})}[\log R(\mathbf{C}, \mathbf{Z})] + \mathbb{E}_{R(\mathbf{Z}, \mathbf{C})}[\log S(\mathbf{C}|\mathbf{Z})]. \quad (11)$$

The first term  $\mathbb{E}_{R(\mathbf{Z}, \mathbf{C})} \log f(\mathbf{X}, \mathbf{Z})$  which represents the observed joint densities of  $\mathbf{X}$  and  $\mathbf{Z}$  is written in the prior section in Eq. (8). The second term  $\mathbb{E}_{R(\mathbf{Z}, \mathbf{C})}[\log R(\mathbf{C}, \mathbf{Z})]$  represents the joint distribution of the two-tiered variational variables and is written as:

$$\mathbb{E}_{R(\mathbf{Z}, \mathbf{C})}[\log R(\mathbf{Z}, \mathbf{C})] = \sum_i \sum_q \tau_{iq} \log \tau_{iq} + \sum_q \left( P_q \log P_q + (1 - P_q) \log(1 - P_q) \right).$$

The third term  $\mathbb{E}_{R(\mathbf{Z}, \mathbf{C})}[\log S(\mathbf{C}|\mathbf{Z})]$  described by Ranganath et al. as the ‘recursive variational approximation’ [53] for  $R(\cdot)$ , can be written as

$$\mathbb{E}_{R(\mathbf{Z}, \mathbf{C})} \log S(\mathbf{C}|\mathbf{Z}) = \sum_i \sum_q \left( P_q \log \Psi + (1 - P_q) \log(1 - \Psi) \right) \tau_{iq}.$$

Combining these elements together, the hierarchical ELBO can be rewritten as:

$$\begin{aligned} \mathcal{L}' = & \mathbb{E}_{R(\mathbf{Z}, \mathbf{C})}[\log f(\mathbf{X}|\mathbf{Z})] + \sum_{i,q} \tau_{iq} \log \alpha_q + \sum_q \sum_i \tau_{iq} \log \tau_{iq} \\ & + \sum_i \sum_q \left( P_q \log \Psi + (1 - P_q) \log(1 - \Psi) \right) \tau_{iq} \end{aligned}$$

The hierarchical ELBO written in full can be found in Appendix B.2. Derivations for all of these terms can be found in Appendix B.3.

## 4 Estimation Algorithm

We summarize the targets of inference here to set up the language for the rest of the section. We distinguish *variational* and *model parameters*: variational parameters  $\tau_q$  and  $P_q$ , for  $q$  from 1 to  $Q$  describe the membership probabilities, while model parameters describe the parametric qualities of the blocks. Within the set of model parameters, we further distinguish *local* and *global* parameters. *Local* parameters are those that pertain to unique blocks indexed by  $q$ : which are described as  $\Theta = \{\alpha, \Theta_{\text{Signal}}\}$  defined in Equation (9).  $\Theta$  is comprised of the means  $\mu_q$ , variances  $\Sigma_q$ , and membership probabilities  $\alpha_q$  for each  $q$ . *Global* parameters are  $\Psi, \Theta_{\text{Noise}}$ . We use Variational EM to estimate variational parameters in the E-step and model parameters in the M-step, alternating these steps until the differences in  $\tau_{iq}$  become miniscule. We present the closed-form solutions to all the estimates below, but more detailed derivations for every term can be found in Appendix C.

### 4.1 E-Step

The E-Step of the algorithm estimates the variational variables which represent block memberships  $Z_{iq}$  of the nodes  $i$  as well as  $C_q$  which are analogous to the ‘memberships of memberships’. First we describe the estimation procedure for the variational approximations  $\tau_{iq}$ , next we describe the estimation of noise-block designation approximations  $P_q$ . This two-step procedure differs from prior work because an additional hierarchical estimation step of the higher-level variational variables  $P_q$  is added.

#### 4.1.1 Estimation of Membership Vectors $\tau$

A iterative fixed-point approach is used to estimate  $\tau_{iq}$ , wherein the derivative for each  $\tau_{iq}$  is taken based on model parameters and  $\tau_{jl}$ . This is the same approach as most existing literature [23, 43]. We use the notation  $f(X_{ij}^k, \mu_q, \Sigma_q)$  to represent the multivariate normal density for edge  $i, j$  with mean  $\mu_q$  and covariance matrix  $\Sigma_q$  at layer  $k$ , and  $f(X_{ij}^k, \mu_{AN}, \Sigma_{AN})$  as the multivariate normal density for observations (observed edges) housed in either interstitial noise  $IN$  or noise block  $NB$ .

$$\begin{aligned} \log(\tau_{iq}) \propto & \log(\alpha_q) + \sum_k \sum_j \tau_{jl} \left( P_q f(X_{ij}^k, \mu_q, \Sigma_q) + (1 - P_q) f(X_{ij}^k, \mu_{AN}, \Sigma_{AN}) \right. \\ & \left. + \sum_{l:l \neq q} f(X_{ij}^k, \mu_{AN}, \Sigma_{AN}) \right) - 1 + P_q \log \Psi + (1 - P_q) \log(1 - \Psi), \end{aligned}$$

then after exponentiating, the fixed-point equation can feasibly be solved after the iterating the system until relative stability. The other variational variables  $P_q$  are calculated as follows:

$$\widehat{P}_q = 1 - \left( 1 + \left[ \exp \left( \sum_k \sum_{i,j} \tau_{iq} \tau_{jq} \left( f(X_{ij}^k, \boldsymbol{\mu}_q, \boldsymbol{\Sigma}_q) - f(X_{ij}^k, \boldsymbol{\mu}_{AN}, \boldsymbol{\Sigma}_{AN}) \right) + \log \left( \frac{1 - \Psi}{\Psi} \right) \right) \right]^{-1} \right)^{-1}. \quad (12)$$

Calculations for each of these terms are provided in the Appendices C.1 and C.2.

## 4.2 M-Step

Similar to its estimation estimates in Daudin et al. [23],  $\alpha_q$  are estimated as follows using Lagrangian multipliers

$$\hat{\alpha}_q = \frac{\sum_{i,q} \tau_{iq}}{n}.$$

The closed-form estimate for the *local* parameters for the mean vector  $\boldsymbol{\mu}_q$  for each block  $q$  from the M-step is

$$\widehat{\boldsymbol{\mu}}_q = \frac{\sum_{i,j} \tau_{iq} \tau_{jq} \mathbf{X}_{ij}}{\sum_{i,j} \tau_{iq} \tau_{jq}} P_q + \boldsymbol{\mu}_{AN} (1 - P_q).$$

In the above, and all subsequent expressions in this subsection, the derivations are located in Appendix C.3. Similarly to mean calculations, the variance calculations (along diagonals) are

$$\widehat{\boldsymbol{\Sigma}}_q = \frac{\sum_{i,j} \tau_{iq} \tau_{jq} (\mathbf{X}_{ij} - \boldsymbol{\mu}_q)^2}{\sum_{i,j} \tau_{iq} \tau_{jq}} \cdot P_q + \boldsymbol{\Sigma}_{AN} \cdot (1 - P_q).$$

The cross-term for two layers  $h, k$  is written as:

$$\widehat{\boldsymbol{\Sigma}}_{hk,q} = \frac{\sum_{i,j} \tau_{iq} \tau_{jq} (X_{ij}^k - \boldsymbol{\mu}_{q,k}) ((X_{ij}^h - \boldsymbol{\mu}_{q,h}))}{\sum_{i,j} \tau_{iq} \tau_{jq}} P_q$$

The element-wise correlations at iteration  $t$  across layers  $h, k$  ( $h \neq k$ ) are then calculated, and the maximum (if  $K > 2$ ) of these values is taken as the putative correlation (across all layers) for block  $q$

$$\hat{\rho}_q = \max_{h,k} \frac{\widehat{\Sigma}_{hk}^q}{\sqrt{\widehat{\Sigma}_q^h \widehat{\Sigma}_q^k}}.$$

If  $K = 2$  then no maximum needs to be taken. This is an operational step of the optimization and does not necessarily yield closed-form estimates. However, we note that this value is the identical to the *mutual coherence* of estimated correlation matrix, as such it serves as a summary statistic of the estimates for correlations that is consistent with the approximation of the convex optimization problem we solve with VEM [56]. Theoretical properties of these relationships should be explored in future work.

### 4.2.1 Estimation of Global Parameters

To calculate the global parameters, the global noise probability term  $\Psi$  defined previously is

$$\hat{\boldsymbol{\mu}}_{AN} = \Psi \frac{\sum_{j,i} \sum_{l,q:q \neq l} \tau_{iq} \tau_{jl} \mathbf{X}_{ij}}{\sum_{j,i} \sum_{l,q:q \neq l} \tau_{iq} \tau_{jl}} + (1 - \Psi) \frac{\sum_{j,i} \sum_q \tau_{iq} \tau_{jq} (1 - P_q) \mathbf{X}_{ij}}{\sum_{j,i} \sum_q \tau_{iq} \tau_{jq} (1 - P_q)}. \quad (13)$$

The covariance term for global noise, as stated earlier, is zero. The variance of global parameters is similarly calculated as:

$$\hat{\boldsymbol{\Sigma}}_{AN} = \Psi \frac{\sum_{j,i} \sum_{l,q:q \neq l} \tau_{iq} \tau_{jl} (\mathbf{X}_{ij} - \boldsymbol{\mu}_{AN})^2}{\sum_{j,i} \sum_{l,q:q \neq l} \tau_{iq} \tau_{jl}} + (1 - \Psi) \frac{\sum_{j,i} \sum_q \tau_{iq} \tau_{jq} (1 - P_q) (\mathbf{X}_{ij} - \boldsymbol{\mu}_{AN})^2}{\sum_{j,i} \sum_q \tau_{iq} \tau_{jq} (1 - P_q)},$$

The derivation for these expressions are in Appendix C.4.

## 4.3 Stochastic Variational Inference

To speed up computation, we apply stochastic variational inference to calculate the membership parameters  $\tau_{iq}$  and  $P_q$ . We subsample nodes at each step of the E-step in variational EM. Calculating  $\tau_{iq,t}$  and  $P_{q,t}$  comprise two stochastic sub-steps of the E-step at iteration step  $t$ ; we label their stochastic VI estimates as  $\hat{\tau}_{iq,t}$  and  $\hat{P}_{q,t}$ . At each  $t$ , we sample a set of nodes  $M = \{i_1, \dots, i_m\}$  of size  $m$  and their associated edges from graph layers  $\mathbf{X}^1, \dots, \mathbf{X}^K$ . Let  $\tau_{iq,t}^m$  represent the randomly subsampled graph at iteration step  $t$ .

1. (Calculating  $\tau_{iq,t}^m$ ) Performing the partial updating step for  $\tau_{iq,t}^*$  at time  $t$  will iteratively calculate the subsampled membership  $u, v \in M$ :

$$\begin{aligned} \tau_{iq,t}^* \propto \exp \left( \log(\alpha_q) + \sum_{k \leq K} \sum_{j,l \in M} \tau_{jl,t-1} \left( P_q f(X_{ij}^k, \boldsymbol{\mu}_q, \boldsymbol{\Sigma}_q) + (1 - P_q) f(X_{ij}^k, \boldsymbol{\mu}_{AN}, \boldsymbol{\Sigma}_{AN}) \right) \right. \\ \left. + \sum_{l:l \neq q} f(X_{ij}^k, \boldsymbol{\mu}_{AN}, \boldsymbol{\Sigma}_{AN}) \right) - 1 + P_q \log \Psi + (1 - P_q) \log(1 - \Psi). \end{aligned}$$

So now the update step takes the average of the newly calculated  $\tau_{iq,t}^*$  with the previous value

$$\hat{\tau}_{iq,t} = \delta_t \tau_{iq,t}^* + (1 - \delta_t) \hat{\tau}_{iq,t-1}$$

2. (Calculating  $P_{q,t}$ ) The signal probability  $P_q$  is calculated in (12) but with the same subsampled replacements as done in the previous calculation of  $\boldsymbol{\tau}$ . For each time point the new noise probability  $p_{q,t}^*$  is calculated and averaged with the previous noise probability at time  $t - 1$ . The update step is

$$\hat{P}_{q,t} = \delta_t p_{q,t}^* + (1 - \delta_t) \hat{P}_{q,t-1}$$

More details on the setup and assumptions of stochastic VI can be found in Appendix D.

## 5 Empirical Performance and Results

In this section we discuss applications of the proposed method and results. The primary purpose of this section is to demonstrate the validity of the model on synthetic and real data, while the primary case study for PNC psychopathology data will be the focus of the following Section 6. We first describe the setting and results for a simulation study that is used to assess the accuracy and computation time of the algorithm. Following this, we describe applying SBANM to longitudinal US congressional voting data and interpret clustering results in Section 5.2. Finally, we describe the setting and experimental design for applying SBANM to human mobility data (bikeshare networks). These results demonstrate the utility of the proposed method to a variety of data, as well as its ability to glean more insight in a variety of settings.

### 5.1 Synthetic Experiments

In this section we describe the setting and outcome of a simulation study that we design to demonstrate the accuracy and efficacy of the proposed method. We considered networks of sizes  $n = 200$  for trivariate and 500 for bivariate networks. The complexity of the estimation algorithm scales up non-linearly with the increase of nodes and layers, but is more efficient and parsimonious compared to existing methods described in the following Section 5.1.5. Computation time for simulations are feasible even in networks of nodes that number the thousands. This becomes necessary for the primary application for the PNC dataset, of which the sample size for one age subsection (*Youth*) number around 5000.

Firstly, we simulate many networks of small to medium size and then apply the algorithm to faithfully recover their memberships and governing parameters. We generate 50 bivariate (two-layer) networks of  $n = 500$  nodes each, and 50 trivariate (three-layer) networks of 200 nodes and run the SBANM algorithm to demonstrate that the method is able to recover simulated data. Secondly, we simulate a single small network of  $n = 200$  nodes and run the algorithm under several different settings for the estimate of blocks  $Q$  and demonstrate that the model selection procedure is valid. We also assess the computation times of various simulations and compare them to other methods.

#### 5.1.1 Experimental Design of Simulation Model

The basic design of the synthetic experiment is to generate weighted multilayer networks with multivariate Gaussian distributions for each differing block, then to run the algorithm on these simulations. The first goal of the simulation is to demonstrate that the proposed method can faithfully recover generated synthetic data. In all of the simulations outlined above, the simulation procedure follows a similar two-step scheme as follows. In the first step, Gaussian parameters are randomly generated using the fixed *priors*. In the second step, multivariate Gaussian distributions are generated from the parameters obtained in the first step.

The number of blocks  $Q$  is first randomly generated between 3 and 5. Means and variances of each block, as well as the global mean and variance for the ambient noise, are then independently generated from normal distribution (ie. a Gaussian prior for the *hyperparameters*), and a positive correlation coefficient is sampled from a uniform distribution between 0 and 1. The first block of each network is designated as  $NB$  and its



mean and variance follow those of  $AN$ . Group sizes  $n_q$  for each block are generated from a multinomial distribution, which were drawn from Dirichlet priors.

After the ground-truth parameters are generated, we proceed to the second data-generating step. For each mean-covariance pair corresponding to a block, we generate multivariate Gaussian distributions with a sample size of  $n_q(n_q - 1)/2$ , then we plug these multivariate data to the format of weighted edges. Finally, a sample of the  $AN$  distribution with sample size

$$n_{IN} := (n - 1)/2 - \sum_{q:1 \leq q \leq Q} n_q(n_q - 1)/2$$

is generated for all  $n_{IN}$  interstitial edges between differing blocks.

### 5.1.2 Choice of Number of Blocks

*Model selection* in the SBM clustering context usually refers to selection of the number of a priori blocks before VEM estimation as it is the only ‘free’ parameter in the specification step of the algorithm. Existing approaches [23, 43, 44] consider the *integrated complete likelihood* (ICL) for assessing block model clustering performance. Matias et al. write the ICL for multilayer graphs in the following way (adapted to match the notation of this study)

$$ICL(Q) = \log f(\mathbf{X}, \mathbf{Z}) - \frac{1}{2}Q(Q - 1) \log(n(K - 1)) - pen(n, K, \Theta) \quad (14)$$

to translate the terminology,  $\Theta$  corresponds to the total set of transition parameters in the SBM, where  $\Theta := \Theta_{\text{Signal}} \cup \Theta_{\text{Noise}}$  [44]. The penalty parameter  $pen(\cdot)$  is chosen dependent on the distributions of the networks; the ‘Gaussian homoscedastic’ case in Matias et al. is derived to be

$$pen(n, K, \Theta) = Q \cdot \log\left(\frac{n(n - 1)K}{2}\right) + \frac{Q(Q - 1)}{2}K \cdot \log\left(\frac{n(n - 1)}{2}\right).$$

Though the authors made the assumptions that the variances are constant for all blocks, we assume that the models are similar enough to SBANM such that the evaluation criterion is applicable to our case. For this portion of the simulation experiment we fix  $n$  at 200 and the ground-truth  $Q$  at 5. However, we apply the method for a range of hypothesized block numbers  $\hat{Q}$  (as the *estimate* for number of blocks) from 2 to 7. Simulation results show that the usage of ICLs caps at  $\hat{Q} = 5$ , the correct ground truth value.

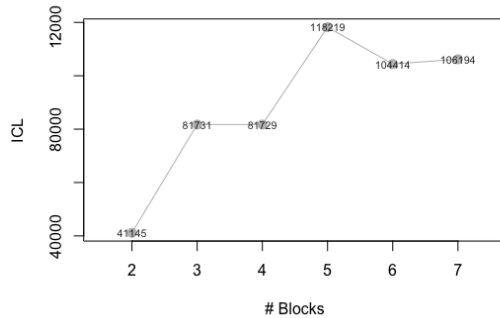


Figure 2: ICLs for simulation study for three-layer network of 200 nodes with a ground-truth  $Q$  of 5, which maps to the maximum ICL that was found by the method of estimation.

### 5.1.3 Experimental Procedure

We describe the procedure for generating and applying the SBANM method to synthetic datasets. To generate the networks, in the bivariate case, the means for each unique block for every network are randomly generated from a Gaussian distribution centered around 0 and 2 respectively for the first and second layers. After the parameters are generated, the observations are simulated from multinormal distributions governed by these parameters. Each network has  $AN$  governing both a single block  $NB$  and interstitial noise  $IN$  that is centered around  $(-1,0)$ . We repeat this procedure for trivariate networks of  $n = 200$  nodes, wherein the Gaussian priors for each (signal) block have means of  $-2, 0, \text{ and } 2$  respectively for first, second, and third layers.

In order to ensure the separability of blocks during simulations, we only select the networks whose blocks' minimum Bhattacharya distances are above a certain threshold. To this end, we calculate the minimum Bhattacharya distances between blocks across 500 simulated networks, and then select the top 10% of the minimum Bhattacharya distances to filter out the networks whose blocks are 'far enough away' from each other. As such, we run 50 instances of the SBANM algorithm for both the bivariate ( $n = 500$ ) and the trivariate case ( $n = 200$ ).

We initialize the algorithm by applying spectral clustering on the sum graph  $\tilde{X}$  across all  $K$  layers, such that each entry on a single flattened graph  $\tilde{\mathbf{X}}$  is  $\tilde{X}_{ij} = \sum_{k=1, \dots, K} X_{ij}^k$ . Another option is drawing that every  $\tau_{iq}$  is drawn from a uniform distribution, then normalized such that each row sums to 1. Matias et al. propose averaging the graphs and then running k-means over the averages [44]. We initialize by first averaging the layers to  $\tilde{X}_{ij}$ , then by using spectral clustering [54], which approximates the community structure in a single network in a fast and reliable way. However, it does not capture the nuanced relationships embedded within the interplay of layers: occasionally, a user may find the need to use an alternative method if the spectral clustering initialization is unsatisfactory, such as sampling from a uniform distribution. In the rest of the manuscript, we also initialize using spectral clustering applications to real data.

### 5.1.4 Experimental Results

Fifty runs of the algorithm were performed for both the (highest minimum Bhattacharya distance) *filtered* and *unfiltered* cases. Among the unfiltered cases, 50 networks were generated at random with the specified hyperparameters with no attention paid to the distances between distributions amongst blocks. In the filtered cases, 500 networks were generated as described in the previous Section 5.1.3, then the networks with the highest 10% of the minimum Bhattacharya Distances are kept for the algorithm to be applied to.

We first examine the *exact recovery* rates of the algorithm (for memberships). We define "exact recovery" to mean whether the SBANM algorithm is able to correctly impute and place all the block memberships of the network that was generated based on the multinormal simulation scheme in Section 5.1.3 [1]. Results show that the top 10% *filtration* procedure for bivariate simulations induces nearly a 100% (49/50) recovery rate; and 70% (37/50) for the trivariate simulations. We note the sensitivity of the recovery rates to the increase in dimensions (or layers); and hints at some parallels with *curse of dimensionality* for community detection in multilayer networks [25]. Increasing dimensions tends to induce more probable mixtures between blocks that are close together.

Parameter estimates are also reasonably retrieved from the **SBANM** algorithm, both in absolute and relative terms. Mean errors are centered around zero as to not show any systemic bias; absolute percentage differences between ground truths and their estimates hover around 10-25%; some of the discrepancies may arise from small ground truth values or imperfectly matching memberships. More details can be found in Appendix G, which includes histograms of parameter estimates and results on larger networks.

### 5.1.5 Comparison with Other Methods

We compared the proposed **SBANM** method with spectral clustering as well as the **dynsbm** proposed by Matias et al. [44]. We applied spectral clustering ‘naively’ as in the initialization scheme where all layers are summed and collapsed into a single network because this is an intuitive simple and fast method for multilayer community detection. When we compare to the method with **dynsbm**, we assume two interpretations of their clustering results. Because **dynsbm** imputes different block memberships for every layer, we convert these into cross-layer persistent community labels by (1) taking the most frequent occurrence of the clustered membership across all layers and (2) treating each block-combination across layers as a unique configuration for the definition of a new block. This need to interpret the results of **dynsbm** already reveals an implicit advantage of the **SBANM** method in its inherent parsimony of clusters and interpretability of blocks across layers for certain fitting data-types and scientific questions.

We evaluated *ARI* (Adjusted Rand Index) and *NMI* (Normalized Mutual Information) scores [44, 49, 59]. for the three methods with the 50 simulations for both bivariate and trivariate networks and have found that **SBANM** outperforms competing methods in every setting. In the bivariate case, because nearly all simulations yielded *perfect recovery*, the *NMI* and *ARI* are both very close to 1. In the trivariate case, the high *NMIs* and *ARIs* suggest effective *partial recovery* of the memberships if some of the network block structures are not perfectly recovered. We note that none of the competing methods perfectly recover the block structures for entire networks. We also note that spectral clustering in the bivariate case outperforms **dynsbm**, but not in the trivariate case; suggesting a potential sensitivity of spectral clustering to the curse of dimensionality.

Computing times were higher in **dynsbm** compared to **SBANM** (for spectral clustering, computing time is nearly instant) in both bivariate and trivariate cases. In trivariate cases, the mean time for trivariate cases (with 200 observations each) is 144 seconds with SD of 548, compared to 160 (SD 125) seconds on average for **dynsbm**. Though **SBANM** computing times have fairly high variance, it is comparable in time to that of **dynsbm** in the trivariate cases. The time differential is much larger in larger bivariate networks. The mean time was 330 seconds (SD 328) for **SBANM** and on average 859 (SD 88) seconds for a few samples of **dynsbm**. The time difference in computation suggests that **SBANM** may better handle larger-size graphs than existing methods. Fitting larger networks when  $n > 5000$  are feasible for **SBANM**, but not for **dynsbm**.

## 5.2 US Congressional Voting Analysis

The overarching motivation for this application is belied by the assumption that political parties change over time and do not necessarily capture the political “tribes” in the US House of Representatives in the past and the present. Prior work use co-voting patterns in the congress and senate in the United States to demonstrate applications of multilayer

METHOD COMPARISON				
<b>Bivariate (50 Runs)</b>				
<i>Method</i>	<i>NMI</i>		<i>ARI</i>	
	Mean	SD	Mean	SD
SBANM	1.00	0.02	1.00	0.01
Spectral	0.80	0.27	0.84	0.24
dynsbm (unique config.)	0.62	0.25	0.67	0.25
dynsbm (most freq.)	0.68	0.25	0.71	0.25
<b>Trivariate (50 Runs)</b>				
<i>Method</i>	<i>NMI</i>		<i>ARI</i>	
	Mean	SD	Mean	SD
SBANM	0.87	0.26	0.87	0.27
Spectral	0.65	0.31	0.69	0.29
dynsbm (unique config.)	0.75	0.21	0.80	0.21
dynsbm (most freq.)	0.70	0.16	0.77	0.18

Table 1: Comparison of different methods for membership recovery using the ARI and NMI measures. `dynsbm` (unique config.) refers to the interpretation of the method when every unique configuration of blocks across layers are treated as a unique block. `dynsbm` (most freq.) treats the block with the most frequent occurrence of memberships across all layers as the cross-layer block.

SBMs by representing district representatives (or senators) as nodes and their covoting similarities as edges [19, 58]. Though most congressional seats have fixed political parties that are representative of their political alignments, parties are assemblages of many constituents with issues that often fragment or congeal (ie polarize) over time. As such, it is useful to trace and segment the groups that either vote with each other persistently, or change drastically following some significant demographic shift. Clustering different political ‘tribes’ by their similarities in voting is important for studying and forecasting patterns in US politics. In particular, it may be of interest to look for certain ‘swing’ districts that yield more signal for political analysts to study, compared to the ambient levels of connectivity in politically non-contentious districts.

We procure voting data from *Voteview* [40]. We use data from all congressional line items from the 100th (1987-89), and 115th (2017-19) sessions, excluding consensus votes where all votes were ‘yes’ or ‘no’. These sessions sample distinct decadal political milieus in the United States across 30 years and serve as snapshots indicating long-term changes in the political inclinations of congressional districts. Though the number of these districts total 435 presently, differing seats often appear and vanish due to redistricting, and we use the seats that were common to both sessions. The resulting network size  $n$  is 393.

We use similarity measures similar to that which was applied to PNC survey data for voting records. Between two district seats, which are represented by nodes  $i$  and  $j$ , the total votes in agreement (both yes or both no) are summed, then subtracted by the total disagreeing votes and divided by the total votes cast. We convert this correlation-like value, which is between -1 and 1, to a statistic that approximates to a normal distribution by applying the same Fisher transformation used in Section 2. Like in other studies [58], consensus votes that have either 100% ‘yes’ or 100 % ‘no’ are omitted.

We ran the algorithm over a range of values for estimated block numbers  $Q$ , as was done in Section 5.1.3. As the block sizes increase, the ICL also increases, until  $Q := 3$  which is where it appears to attain a maximum. We display the clustering results for 3

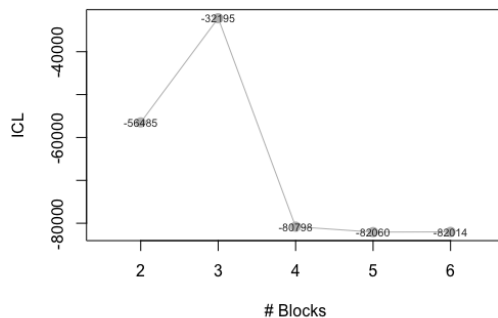


Figure 3: Block selection for US congressional voting data based on the method; 3 blocks yields the greatest ICL.

blocks are shown in Figure 3. In addition to the block sizes and estimated correlations, we show the average percentage of Republican party membership ( $\%R$ ) in the 100th and 115th sessions. The results show capture distinct shifts in party membership across the years:  $NB$  appears to capture the moderate niche of the congress.

MEMBERSHIPS, PARAMETERS, AND PARTY AFFILIATION							
Block	$n$	$\mu_{X,q}$	$\mu_{Y,q}$	$\rho_q$	$\%R(100th)$	$\%R(115th)$	Notable People
$NB$	9	0.02	0.31	0.00	36	67	Nancy Pelosi (1)
$S_1$	233	0.71	0.36	0.09	4	50	Beto O'Rourke(2), Paul Ryan(2)
$S_2$	151	0.55	0.45	0.04	99	68	Dick Cheney(1), Liz Cheney(2)

Table 2: Clustering results for congressional voting data in the 100th and 115th sessions. In addition to the means and correlations of the (normalized) similarity networks, mean (Republican) party membership rates and notable people in each block are given.

Nine members in  $NB$  vote at the same rate with each other as with any other cluster; The interpretation of this block as *moderate* is supported by membership of *moderate Democrat* politicians such as Nancy Pelosi who occupied the seat during empirically verified by the fact that more than half of the block is Republicans in the 115th session. Moreover,  $NB$  yields the same rate as every other block votes at the same rate with a different block.

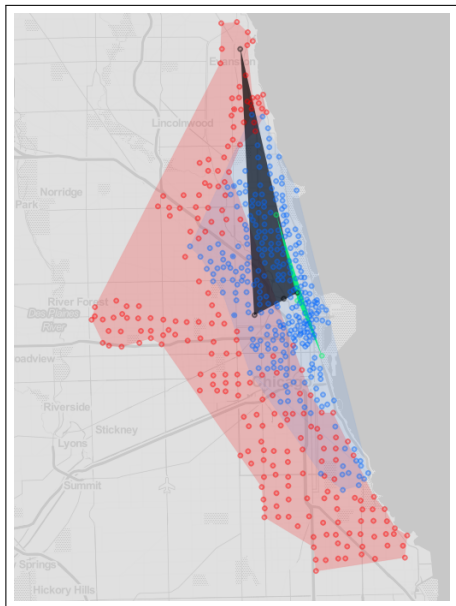
The two biggest political enclaves are large bipartisan *party* that is half Democrat and half Republican in 2015 but was almost entirely Democrat in 1987 ( $S_1$ ), and another group that was almost entirely Republican in 1987 but only about 2/3 Republican in more recent times. The asymmetry in the blocks  $S_1$  and  $S_2$  is perhaps of note; one can view possibly  $S_2$  as analogous to  $S_1$ , but more likely the block is capturing an uneven relationship where there is no Democratic equivalent to the Republican block  $S_2$  which shows entrenchment of voting ideology along geographical (district-wise) lines. These dynamics may be due to fundamental differences in voting patterns between the two parties. Results reveal the large drop-off in the Democrats' political dominance in the 100th session. Instead of capturing static (same-period) blocks, SBANM is able to capture some of the largest *differential* movements between the 1980s and 2015.

### 5.3 Human Mobility Data Analysis

The SBANM method is applicable to human mobility patterns which is represented by bikeshare data. Bikeshare networks have been argued to trace the latent patterns within

human mobility in urban systems [18]. He et al. [28] and others have modeled bikeshare stations as nodes and aggregate trips as edges [17], and then gathered conclusions about the patterns of human mobility within these bike-sharing constraints. In particular, prior work have analyzed differences in time-of-day patterns, functional differences (ie work-to-home and home-to-home trips), as well as long-term usage between neighborhoods. Carlen et al. have proposed a time-dependent SBM for (binary) paths between bikeshare stations [17]. We convert trip data from the public records of the *Divvy* bikeshare system into time-series networks where each edge represents trips and each node represents stations. We write these network time-series as  $\{G_s\}_{1 \leq s \leq S}$ , where  $S$  is the aggregate weekly time-points between January 2014 to June 2016, and  $\{G_t\}_{1 \leq t \leq T}$  for  $T$  as the aggregate weekly time-points between July 2016 to December 2018, as was done a previous analysis of the *Divvy* system as conducted in He et al. [29]. New stations as well as stations that were removed during this time are omitted, such that the total number of stations ( $n = 547$ ) is consistent across time.

We sum all of the edges across all time points for distinct time-periods  $S$  and  $T$ . The two graphs  $\mathbf{X}$  and  $\mathbf{Y}$  represent differential layers across two temporal regimes. We use the number of aggregated trips across each time-regime  $\mathbf{X}$  and  $\mathbf{Y}$  to represent edge-weights. The edge-weights are then transformed by dividing each value by the respective strengths (sum of weights) to procure a ratio between 0 and 1. The ratio is then converted into an approximately normal value by the *logit* transformation. Because of this transformation, mean values are negative and between -10 and -20. Estimated statistics (Figure 4) are reconverted using the inverse logit transform, then multiplied by the total graphwise sum-of-strengths, to convey a normalized mean rate of trips across stations within the same community.



PARAMETER ESTIMATES					
		$n$	$\mu_X$	$\mu_Y$	$\rho_q$
●	NB	4	1.22	0.37	0
●	$S_1$	216	8.48	4.78	0.67
●	$S_2$	3	17.1	0.21	0.00
●	$S_3$	295	0.29	0.26	0.87

Figure 4: *Communities found across 2 time-periods in the Divvy Bikeshare networks in Chicago, with associated (normalized) estimates for (normalized) mean rates of trips within the cluster in each time period, as well as correlations.*

Results show distinct geographical patterns (Figure 4). The red cluster is the largest (at 295 nodes) and represents a distinct baseline group for both time periods with activity

that persist across time. The high inter-block correlation of .87 in this block suggests persistent trip interactions across time. The blue cluster represents a smaller (216 nodes) but a more *persistent* area of activity: it has higher means for both the first and second layers than that of  $S_1$  for both time-regimes, and also has a high correlation rate. Because this area is closer to more affluent areas around the lake with more parklike amenities (such as the lakefront bike path), this block signifies zones with higher trip activity across both time periods.

Smaller groups  $NB$  and  $S_2$  concentrate around the northern part of the city and have very different estimated means that signal drastic change in usage over time. Indeed, the green block  $S_2$  has the highest first-layer mean  $\mu_X$  but the lowest second layer mean  $\mu_Y$ . That the correlation in this block across layers is zero furthermore suggests a disjointly decreased usage over the two time periods.  $NB$  is represented by the grey-black cluster in the northwest part of the city and has the same parameters of ridership as riders traversing across different blocks; which offers an interpretation to the large, but not infeasible, distance between stations (members) in this block. These discovered clusters have interpretable results and suggests the viability of the method to human mobility data, after the appropriate transformations.

## 6 Case Study: PNC Psychopathology Networks

After validating the method on simulations and real-world datasets, we apply SBANM to the PNC data which constitutes the primary case study of this paper. We use networks constructed from *anxiety*, *behavior*, and *mood* psychopathology surveys as described in Section 2, and then validate the discovered communities from clinical diagnoses for each disorder as well as typical development (TD) and psychosis. We let  $\mathbf{X}^x$  represent the network of symptom response similarities for anxiety,  $\mathbf{X}^y$  for behavior, and  $\mathbf{X}^z$  for mood disorders. Correspondingly, we let  $(\mu_x, \mu_y, \mu_z)_{q:1 \leq q \leq Q}$  represent the means of the edge-connections for each block representing anxiety, behavior, and mood with corresponding standard deviations  $(\sigma_x, \sigma_y, \sigma_z)_{q:1 \leq q \leq Q}$ .

To the best of our knowledge, not much prior work has approached the study of psychiatric networks by constructing networks of individuals as nodes and their similarity as edges. The primary focus of applying the SBM with ambient noise to psychopathology symptom data is to identify groups of people who have similar clinical characteristics and facilitating early identification of individuals who could be at high risk. Existing classification studies on psychosis typically require input (or “training on”) from already-diagnosed subjects, or psychosis specific symptoms. These methods usually use methods such as logistic regression or support vector machines [16]. However, we aim to classify anxiety, mood, and behavior symptoms to identify who is at risk for psychosis without the use of psychosis labels in a sample of youth aged 8-21 years, a developmental period prior to the onset of psychotic disorders. Conducting such an unsupervised study would be clinically advantageous in early identification.

We ran the method on youth and early adult data under several different specifications for number of blocks  $Q$ . We applied the method to data on 5136 youth under  $Q = 3$  and 4 fixed blocks. We ran the method for the *early adult* data (1863 subjects) for  $Q = 4$  and 5. In each of these runs the SBANM algorithm has separated the population into distinct groups with varying block sizes. Table 3 shows that for all choices of  $Q$ , highly correlated blocks and  $NB$  are discovered with ample separation in terms of Bhattacharya distances. Memberships of blocks range from only a few subjects to several hundred.

Parameter Estimates														
Block	$n$	$\rho_q$	$\mu_x$	$\sigma_x$	$\mu_y$	$\sigma_y$	$\mu_z$	$\sigma_z$	$d(N)$	$d(S_1)$	$d(S_2)$	$d(S_3)$	$d(S_4)$	
<b>Youth: 4 Groups</b>														
● $NB$	247	0	-0.8	0.4	-0.6	0.5	-0.3	0.4	0.0	1.7	0.4	3.9		
● $S_1$	2552	0.30	-1.1	0.3	-1.0	0.5	-1.4	0.2	1.7	0.0	0.7	3.8		
● $S_2$	852	0.51	-0.7	0.3	-0.2	0.2	-0.4	0.1	0.4	0.7	0.0	1.5		
● $S_3$	1485	0.71	-0.6	0.3	-0.6	0.4	0.1	0.3	3.9	3.8	1.5	0.0		
<b>Youth: 3 Groups</b>														
● $NB$	408	0	-0.8	0.3	-0.5	0.4	-0.5	0.3	0.0	3.2	0.5			
● $S_1$	2552	0.30	-1.1	0.3	-1.0	0.5	-1.4	0.2	3.2	0.0	1.7			
● $S_2$	2176	0.51	-0.6	0.3	-0.5	0.4	-0.0	0.3	0.5	1.7	0.0			
<b>Early Adult: 5 Groups</b>														
● $NB$	128	0	-0.6	0.4	-0.4	0.5	-0.4	0.4	0.0	74.4	0.5	1.8	0.9	
● $S_1$	2	0.04	-1.5	0.0	-1.9	0.0	0.4	0.0	74.4	0.0	79.6	125	141	
● $S_2$	338	0.55	-0.2	0.2	-0.1	0.1	-0.3	0.2	0.5	79.6	0.0	4.6	1.9	
● $S_3$	792	0.61	-0.9	0.5	-0.7	0.5	-1.4	0.2	1.8	125	4.6	0.0	4.2	
● $S_4$	603	0.74	-0.7	0.3	-0.5	0.4	0.1	0.4	0.9	141	1.9	4.2	0.0	
<b>Early Adult: 4 Groups</b>														
● $NB$	48	0	-0.2	0.1	-0.1	0.2	-0.2	0.7	0.0	2.3	0.4	2.2		
● $S_1$	1495	0.49	-0.9	0.3	-0.7	0.5	-0.6	0.5	2.3	0.0	0.7	2.3		
● $S_2$	39	0.56	-0.2	0.1	0.1	0.1	-0.4	0.5	0.4	0.7	0.0	1.4		
● $S_3$	281	0.64	-0.1	0.1	-0.1	0.1	-0.4	0.5	2.2	2.3	1.4	0.0		

Table 3: Estimated parameters between blocks in youth and early adult subjects, as well as Bhattacharya distances between the blocks. Mean rates for anxiety response networks are represented by  $\mu_x$ , behavior  $\mu_y$ , and mood  $\mu_z$ . Associated standard deviations are also shown.

We used the ICL procedure from Sections 5.1 and 5.2 to select for the optimal block sizes. For youth, the ICL higher for the results when  $Q = 3$  than for  $Q = 4$ , signifying preferable model for three-block model. In the early adult cohort, the ICL is higher when  $Q = 4$  compared to when  $Q = 5$ . In both youth and early adults, the ICLs suggest that the more parsimonious selections are preferable. In the remainder of this section we mostly focus on the results of these selections of  $Q$ , unless there are results specific to the suboptimal- $Q$  model. However, we also note results across model specifications: for example, in youth the same 2552-member cluster is persistent in both settings for  $Q$  (3 and 4) (Table 3). These results show the persistence of the constellation of symptom agreements across mood, behavior, and anxiety layers.

In general, these results demonstrate the ability of SBANM to integrate *anxiety*, *mood*, and *behavior* symptoms to differentiate groups that signal differential behaviors. Table 4 shows the average rates of positive symptoms for various conditions from clinical diagnoses. The leftmost columns after block labels and sizes are positive indicators for anxiety, behavior, and mood disorders. They are distinct from symptom data in that each indicator is a simple binary ‘yes’ or ‘no’ for each subject. In nearly all the clustering results, the rates of psychosis spectrum is clearly differentiated among differing clusters. Among youth subjects,  $S_1$  correspond to a group that has relatively low incidence of psychosis (13%) (in both choices of  $Q$ ). However,  $S_2$  exhibit similar, almost identical qualities with the same rates of psychosis spectrum, despite having different block-sample sizes.

In youth subjects, the  $S_1$  group (in yellow) appears to be have the highest rates of typically developing (TD) youth (Table 4). This observation holds for both 3 and 4 groups, as the groups are identical. This group could broadly be demarcated as a relatively *normal* group. Though it appears that there are similar rates of TD and psychosis spectrum for  $NB$  and  $S_3$ , further analysis show that the subjects indexed in  $S_3$  have higher rates of



psychosis symptoms in general for youth. In early adults, the higher rates of psychosis symptoms are indexed in the  $NB$ . Such differences warrant further examination with a nuanced discussion and is the focus of a clinical manuscript currently in preparation. The ambient noise  $AN$  is identical for those that in the  $NB$  group as well as inter-block edges  $IN$ . Because it models all between-block interactions,  $NB$  in this context may be better interpreted as a ‘mean’ group characteristics that straddles those who exhibit psychosis spectrum symptoms and those who do not. In the context of a sample that is part symptomatic and part “control” with absence of symptoms,  $NB$  may be interpreted a number of different ways. That the symptoms are uncorrelated across all layers, and potentially signal groups that tend towards psychosis through more individuated channels.  $NB$  contrast with  $S$  blocks wherein  $\mathbf{X}^x$ ,  $\mathbf{X}^y$ , and  $\mathbf{X}^z$  are all strongly correlated with each other.

Psychopathology Symptoms							
Block	$n$	Anx	Beh	Mood	TD	Psy	
<b>Youth: 4 Groups</b>							
●	$NB$	247	56	50	30	7	44
●	$S_1$	2552	37	30	1	44	13
●	$S_2$	852	61	72	18	9	39
●	$S_3$	1485	64	51	29	15	44
<b>Youth: 3 Groups</b>							
●	$NB$	408	52	71	14	10	36
●	$S_1$	2552	37	30	1	44	13
●	$S_2$	2176	64	55	27	13	44
<b>Early Adult: 5 Groups</b>							
●	$NB$	128	61	44	45	9	25
●	$S_1$	2	0	0	100	0	0
●	$S_2$	338	51	28	16	33	29
●	$S_3$	792	41	15	1	50	7
●	$S_4$	603	69	37	44	15	33
<b>Early Adult: 4 Groups</b>							
●	$NB$	48	56	52	40	23	56
●	$S_1$	1495	59	28	23	28	19
●	$S_2$	39	31	33	5	44	31
●	$S_3$	281	25	10	7	60	21

Table 4: Mean summary statistics for psychiatric diagnoses. The following columns details symptoms of anxiety, behavior, and mood disorders. The ‘Psy’ column gives the average of whether the respondents have overall diagnoses for psychosis.

In early adult subjects,  $NB$  appears to have higher rates of psychosis on average. When  $Q$  is 4,  $NB$  actually maps to the group with the highest rates of psychosis, as well as the lowest rates of TD subjects. When  $Q = 5$ , however,  $S_3$  appears to map to a more typical group (with 50% TD and 7% psychosis). This cluster (for early adults) mirrors the  $S_1$  group found in youth results; and does not seem to appear when  $Q$  is set to 4.

The differential clustering results for youth and early adults potentially hints at latent neurodevelopmental pathways for onset of psychosis. Onset of psychosis is characterized by presence of active psychotic symptoms and occurs during early adulthood. Psychosis onset is also better understood as a continuum with psychosis patients reporting proportionally more nonpsychotic symptoms (such as depression and anxiety among others) prior to the onset of psychosis [22]. As symptoms segregate with growth and development psychopathology symptom relationships potentially become statistically more independent.

Results did not show any strong differentiation in demographic characteristics: rates

of patients who are African American, Hispanic, or female roughly were even across the board for most clusters for both youth and early adult under different  $Q$  specifications. Regression Z-scores (with respect to psychosis) of demographic factors do not appear to be significant for any cluster (Table 5 in Appendix H).

## 7 Discussion

We have introduced a novel method that is motivated by real-world clinical problems and that offers a data-driven approach for grouping subject psychopathologies that may predicate deeper understanding or even discovery of psychosis and schizophrenia based on the principles of statistical network theory. We demonstrated the relative efficacy and accuracy of this model compared to existing community detection algorithms.

Network data in recent years come in more complex forms, which map to the variegation of ways that data interact and relate with one another. and are particularly synchronous with the rise of availability in more different types of data, with even more complex configurations of community structures. Our primary contribution in this research was to introduce the notion of structured noise to weighted SBMs. The noise block  $NB$  implicitly constrains and makes parsimonious the proposed model. Other work has explored cases where between-block transitions are all uniquely parameterized [44], but they do not account for correlations between layers nor do they separate signal from noise). The proposed model is more parsimonious, and reveals more useful and more realistic results in clinical and experimental settings. More details on this parsimony can be found in Appendix F. In practice,  $NB$  does not usually represent a control group but rather a volatile or dynamic group that reflect the noisiest interactions. These results are intuitively consistent as the background noise that captures all inter-group relationships are more *abnormal* than *normal*. Typically, however, a block that represents control cases does emerge in applications. In PNC data, a large block persistently espouses the lowest psychosis and highest TD rates.

We have demonstrated that the method is able to uncover latent, non-trivial patterns in domains as disparate as psychiatry, politics, and human mobility. The application of SBANM to psychopathology data, in particular, reflects an ongoing discourse around the notion of *nosology* wherein psychiatric disorders are treated as discrete entities as opposed to multifaceted, multimodal configurations of pathologies [57]. Ontologically, the proposed methodology reinforces the notion that more holistic diagnoses for psychiatric conditions may be more suitable for modern practice.

Despite its numerous advantages, there remain limitations with SBANM. The issue of computation time persistently plagues SBM estimation using VEM, or any kind of methodology involving iterative computational procedures. The algorithm seems to slow down when  $K$  or  $Q$  is large. However, in practice it outperforms existing methods, partly because of its inherently parsimonious nature. Moreover, usage of stochastic VI has sped up computation time such that previously infeasible sample sizes are made possible. Future work may further explore subsampling methods similar to stochastic variational inference to induce faster computation times.

*Ambient noise* in networks dovetail the notion of overlapping communities and in particular, SBMs. A class of community detection methods adhere to a *bottom-up* heuristic where sets are small at first gradually increase in size until memberships become stable; and naturally allows for separation between, *signal* and *noise*. Many of these approaches

implicitly assume inherent structure but do not assign an explicitly parametric model to signal or noise [11, 49, 59]. Members not assigned to communities are called *background* nodes are identified but not statistically modeled. Uncertainty and ambiguity in block-memberships may be represented by either *noise* or *overlapping blocks*. Mixed membership blockmodels have been very useful in modeling real-world data. However, in multilayer graphs, overlaps in high dimensions lead to more problems of parameter identifiability (or altogether avoided [42]), and a natural byproduct effect of ambient noise serves to assuage the “curse of dimensionality”. We refer the reader to the work of Latouche et al. and Airoldi et al. [2, 39] for background on overlapping SBMs, and leave the connection between *representing noisy signals via overlapping memberships* and global *ambient noise* to future work. Theoretical properties of the model relating to dimensional sensitivities, particularly pertaining to minimum Bhattacharya distances between blocks as was investigated in the simulations, should also be explored in future work.

The development of **SBANM** opens up a bevy of potential methodological avenues. One immediate next step is to expand the study of PNC data to neuroimaging and genomics data. Such work is currently in progress for the PNC study to identify potentially jointly causal neural genetic influences in addition to clinically relevant symptoms. Another direction is in assessing significance of connectivity in SBM fits (in general) that leads to the issue of hypothesis testing on SBMs. One augmentation to **SBANM** is to differentially account for whether blocks across layers are significantly connected or different across blocks *or* layers. More generally, these models for in-group and out-of-group interactions feed into the notion of mixed effects models for multimodal weighted networks that may serve as a network-theoretic extension of longitudinal analysis.

## Reproducibility

Code and sample data for the **SBANM** method is available on <https://github.com/markhe1111/SBANM>.

## Acknowledgements and Funding Information

This project was funded by the Rockefeller University Heilbrunn Family Center for Research Nursing (RX, 2019) through the generosity of the Heilbrunn Family. The funding organizations had no role in the design and conduct of the study; collection, management, analysis, and interpretation of the data; preparation, review, or approval of the manuscript; and decision to submit the manuscript for publication. MH was supported by the NSDEG fellowship.

Philadelphia Neurodevelopment Cohort (PNC) clinical phenotype data used for the analyses described in this manuscript were obtained from dbGaP at <http://www.ncbi.nlm.nih.gov/sites/entrez?db=gap> through dbGaP accession phs000607.v3.p2. Support for the collection of the data for Philadelphia Neurodevelopment Cohort (PNC) was provided by grant RC2MH089983 awarded to Raquel Gur and RC2MH089924 awarded to Hakon Hakonarson. Subjects were recruited and genotyped through the Center for Applied Genomics (CAG) at The Children’s Hospital in Philadelphia (CHOP). Phenotypic data collection occurred at the CAG/CHOP and at the Brain Behavior Laboratory, University of Pennsylvania.

The authors thank Andrew Nobel and Shankar Bhamidi for helpful comments and theoretical advice. In particular, we thank them for defining and recognizing the problem of differential, correlated communities amongst multilayer networks.

## References

- [1] Abbe, E. (2017). Community detection and stochastic block models: recent developments.
- [2] Airoldi, E. M., D. M. Blei, S. E. Fienberg, and E. P. Xing (2007). Mixed membership stochastic blockmodels.
- [3] Allman, E. S., C. Matias, and J. A. Rhodes (2009, Dec). Identifiability of parameters in latent structure models with many observed variables. *The Annals of Statistics* 37(6A), 3099–3132.
- [4] Allman, E. S., C. Matias, and J. A. Rhodes (2011, May). Parameter identifiability in a class of random graph mixture models. *Journal of Statistical Planning and Inference* 141(5), 1719–1736.
- [5] Ambroise, C. and C. Matias (2010). New consistent and asymptotically normal estimators for random graph mixture models.
- [6] Association, A. P. (2013). *Diagnostic and statistical manual of mental disorders: DSM-5* (5th ed. ed.). Washington, DC: Autor.
- [7] Bender, E. and A. Canfield (1978). The asymptotic number of labeled graphs with given degree sequences. *Journal of Combinatorial Theory, Series A* 24(3), 296–307.
- [8] Bickel, P. J. and A. Chen (2009). A nonparametric view of network models and newman–girvan and other modularities. *Proceedings of the National Academy of Sciences* 106(50), 21068–21073.
- [9] Blei, D. M., A. Kucukelbir, and J. D. McAuliffe (2017). Variational inference: A review for statisticians. *Journal of the American Statistical Association* 112(518), 859–877.
- [10] Blevins, A. S., J. Z. Kim, and D. S. Bassett (2021). Variability in higher order structure of noise added to weighted networks.
- [11] Bodwin, K., K. Zhang, and A. Nobel (2015). A testing-based approach to the discovery of differentially correlated variable sets.
- [12] Bollobás, B. (1980). A probabilistic proof of an asymptotic formula for the number of labelled regular graphs. *European Journal of Combinatorics* 1(4), 311–316. `bibtex[publisher=Academic Press]`.
- [13] Calkins, M. E., K. R. Merikangas, T. M. Moore, M. Burstein, M. A. Behr, T. D. Satterthwaite, K. Ruparel, D. H. Wolf, D. R. Roalf, F. D. Mentch, H. Qiu, R. Chiavacci, J. J. Connolly, P. M. Sleiman, R. C. Gur, H. Hakonarson, and R. E. Gur (2015). The philadelphia neurodevelopmental cohort: constructing a deep phenotyping collaborative. *Journal of Child Psychology and Psychiatry* 56(12), 1356–1369.
- [14] Calkins, M. E., T. M. Moore, K. R. Merikangas, M. Burstein, T. D. Satterthwaite, W. B. Bilker, K. Ruparel, R. Chiavacci, D. H. Wolf, F. Mentch, H. Qiu, J. J. Connolly, P. A. Sleiman, H. Hakonarson, R. C. Gur, and R. E. Gur (2014). The psychosis spectrum in a young u.s. community sample: findings from the philadelphia neurodevelopmental cohort. *World Psychiatry* 13(3), 296–305.

- [15] Calkins, M. E., T. M. Moore, T. D. Satterthwaite, D. H. Wolf, B. I. Turetsky, D. R. Roalf, K. R. Merikangas, K. Ruparel, C. G. Kohler, R. C. Gur, and R. E. Gur (2017, February). Persistence of psychosis spectrum symptoms in the philadelphia neurodevelopmental cohort: a prospective two-year follow-up. *World psychiatry : official journal of the World Psychiatric Association (WPA)* 16(1), 62–76.
- [16] Cannon, T. D., C. Yu, J. Addington, C. E. Bearden, K. S. Cadenhead, B. A. Cornblatt, R. Heinssen, C. D. Jeffries, D. H. Mathalon, T. H. McGlashan, D. O. Perkins, L. J. Seidman, M. T. Tsuang, E. F. Walker, S. W. Woods, and M. W. Kattan (2016). An individualized risk calculator for research in prodromal psychosis. *American Journal of Psychiatry* 173(10), 980–988. PMID: 27363508.
- [17] Carlen, J., J. de Dios Pont, C. Mentus, S.-S. Chang, S. Wang, and M. A. Porter (2019). Role detection in bicycle-sharing networks using multilayer stochastic block models.
- [18] Cazabet, R., P. Borgnat, and P. Jensen (2017, April). Using Degree Constrained Gravity Null-Models to understand the structure of journeys’ networks in Bicycle Sharing Systems. In *ESANN 2017 - European Symposium on Artificial Neural Networks, Computational Intelligence and Machine Learning*.
- [19] Cho, Y.-S., G. V. Steeg, and A. Galstyan (2011). Co-evolution of selection and influence in social networks.
- [20] Clark, L., D. Watson, and S. Reynolds (1995). Diagnosis and classification of psychopathology: challenges to the current system and future directions. *Annual review of psychology* 46, 121–153.
- [21] Clauset, A., M. E J Newman, and C. Moore (2005, 01). Finding community structure in very large networks. *Physical review. E, Statistical, nonlinear, and soft matter physics* 70, 066111.
- [22] Cupo, L., S. V. McIlwaine, J.-G. Daneault, A. K. Malla, S. N. Iyer, R. Joobar, and J. L. Shah (2021, 01). Timing, Distribution, and Relationship Between Nonpsychotic and Subthreshold Psychotic Symptoms Prior to Emergence of a First Episode of Psychosis. *Schizophrenia Bulletin*. sbaa183.
- [23] Daudin, J.-J., F. Picard, and S. Robin (2008, Jun). A mixture model for random graphs. *Statistics and Computing* 18(2), 173–183.
- [24] Divvy (2019). Divvy data.
- [25] Ertöz, L., M. Steinbach, and V. Kumar (2003). Finding clusters of different sizes, shapes, and densities in noisy, high dimensional data. In *SDM*.
- [26] Fortunato, S. and D. Hric (2016, Nov). Community detection in networks: A user guide. *Physics Reports* 659, 1–44.
- [27] Girvan, M. and M. E. J. Newman (2002). Community structure in social and biological networks. *Proceedings of the National Academy of Sciences* 99(12), 7821–7826.
- [28] He, M., J. Glasser, S. Bhamidi, and N. Kaza (2020). Intertemporal community detection in human mobility networks.

- [29] He, M., J. Glasser, N. Pritchard, S. Bhamidi, and N. Kaza (2020, Apr). Demarcating geographic regions using community detection in commuting networks with significant self-loops. *PLOS ONE* 15(4), e0230941.
- [30] Hoff, P. D., A. E. Raftery, and M. S. Handcock (2002). Latent space approaches to social network analysis. *Journal of the American Statistical Association* 97(460), 1090–1098.
- [31] Hoffman, M., D. M. Blei, C. Wang, and J. Paisley (2012). Stochastic variational inference.
- [32] Holland, P. W., K. B. Laskey, and S. Leinhardt (1983). Stochastic blockmodels: First steps. *Social Networks* 5(2), 109 – 137.
- [33] Holme, P. (2015, Sep). Modern temporal network theory: a colloquium. *The European Physical Journal B* 88(9).
- [34] Jaakkola, T. S. (2000). Tutorial on variational approximation methods. In *IN ADVANCED MEAN FIELD METHODS: THEORY AND PRACTICE*, pp. 129–159. MIT Press.
- [35] Kahn, R., I. Sommer, R. Murray, A. Meyer-Lindenberg, D. Weinberger, T. Cannon, M. O’Donovan, C. Correll, J. Kane, J. Van Os, and T. Insel (2015, November). Schizophrenia. *Nature Reviews Disease Primers* 1.
- [36] Karrer, B. and M. E. J. Newman (2011, Jan). Stochastic blockmodels and community structure in networks. *Phys. Rev. E* 83, 016107.
- [37] Kendell, R. and A. Jablensky (2003). Distinguishing between the validity and utility of psychiatric diagnoses. *American Journal of Psychiatry* 160(1), 4–12. PMID: 12505793.
- [38] Lancichinetti, A., F. Radicchi, J. J. Ramasco, and S. Fortunato (2011, 04). Finding statistically significant communities in networks. *PLOS ONE* 6, 1–18.
- [39] Latouche, P., E. Birmelé, and C. Ambroise (2011, Mar). Overlapping stochastic block models with application to the french political blogosphere. *The Annals of Applied Statistics* 5(1), 309–336.
- [40] Lewis, Jeffrey B., K. P. H. R. A. B. A. R. L. S. (2020). Voteview: Congressional roll-call votes database.
- [41] Liu, S., S. Wang, and R. Krishnan (2014). Persistent community detection in dynamic social networks. In V. S. Tseng, T. B. Ho, Z.-H. Zhou, A. L. P. Chen, and H.-Y. Kao (Eds.), *Advances in Knowledge Discovery and Data Mining*, Cham, pp. 78–89. Springer International Publishing.
- [42] Liu, W., T. Suzumura, H. Ji, and G. Hu (2018, 04). Finding overlapping communities in multilayer networks. *PLOS ONE* 13(4), 1–22.
- [43] Mariadassou, M., S. Robin, and C. Vacher (2010, 06). Uncovering latent structure in valued graphs: A variational approach. *Ann. Appl. Stat.* 4(2), 715–742.
- [44] Matias, C. and V. Miele (2017). Statistical clustering of temporal networks through a dynamic stochastic block model. *Journal of the Royal Statistical Society: Series B (Statistical Methodology)* 79(4), 1119–1141.

- [45] Menichetti, G., D. Remondini, P. Panzarasa, R. J. Mondragón, and G. Bianconi (2014, 06). Weighted multiplex networks. *PLOS ONE* 9(6), 1–8.
- [46] Newman, M. (2018a). *Networks*. Oxford university press.
- [47] Newman, M. E. J. (2018b, Dec). Estimating network structure from unreliable measurements. *Physical Review E* 98(6).
- [48] Nowicki, K. and T. A. B. Snijders (2001). Estimation and prediction for stochastic blockstructures. *Journal of the American Statistical Association* 96(455), 1077–1087.
- [49] Palowitch, J., S. Bhamidi, and A. B. Nobel (2018). The Continuous Configuration Model: A Null for Community Detection on Weighted Networks. *Journal of Machine Learning Research* 18, 1–48.
- [50] Paul, S. and Y. Chen (2015). Community detection in multi-relational data through restricted multi-layer stochastic blockmodel. *preprint*.
- [51] Paul, S. and Y. Chen (2018). A random effects stochastic block model for joint community detection in multiple networks with applications to neuroimaging. *preprint*.
- [52] Peixoto, T. P. (2018, Jan). Nonparametric weighted stochastic block models. *Phys. Rev. E* 97, 012306.
- [53] Ranganath, R., D. Tran, and D. Blei (2016). Hierarchical variational models. *Proceedings of the 33rd International Conference on Machine Learning*, 18.
- [54] Rohe, K., S. Chatterjee, and B. Yu (2011, 08). Spectral clustering and the high-dimensional stochastic blockmodel. *Ann. Statist.* 39(4), 1878–1915.
- [55] Stanley, N., S. Shai, D. Taylor, and P. J. Mucha (2015). Clustering network layers with the strata multilayer stochastic block model. *CoRR abs/1507.01826*.
- [56] Tropp, J. A. (2006). Just relax: convex programming methods for identifying sparse signals in noise. *IEEE Transactions on Information Theory* 52(3), 1030–1051.
- [57] van Praag, H. M. (2000). Nosologomania: a disorder of psychiatry. *The World Journal of Biological Psychiatry* 1(3), 151–158.
- [58] Wilson, J. D., N. T. Stevens, and W. H. Woodall (2019). Modeling and detecting change in temporal networks via the degree corrected stochastic block model. *Quality and Reliability Engineering International* 35(5), 1363–1378.
- [59] Wilson, J. D., S. Wang, P. J. Mucha, S. Bhamidi, and A. B. Nobel (2014). A testing based extraction algorithm for identifying significant communities in networks. *Annals of Applied Statistics* 8(1), 1853–1891.
- [60] Yan, X., C. Shalizi, J. E. Jensen, F. Krzakala, C. Moore, L. Zdeborova, P. Zhang, and Y. Zhu. (2014). Model selection for degree-corrected block models. *Journal of Statistical Mechanics: Theory and Experiment* 5, 05–07.
- [61] Zhao, Y., E. Levina, and J. Zhu (2012, 08). Consistency of community detection in networks under degree-corrected stochastic block models. *Ann. Statist.* 40(4), 2266–2292.

## A Proofs and Derivations

In this section we provide the proofs and derivations for the terms for the algorithm updates in Section 4.

### A.1 Proof for Hierarchical ELBO

This is a proof paraphrased from Ranganath et al. [53] that the hierarchical ELBO is a sharper lower bound on likelihood than the ELBO.

*Proof.* An inequality can be drawn between the “ordinary” ELBO  $\mathcal{L}$  without any hierarchical information and the Hierarchical ELBO

$$\begin{aligned} \mathcal{L} &= \mathbb{E}_{R_{\text{hv}}(\mathbf{Z})}[\log f(\mathbf{Z}, \mathbf{X})] + \mathcal{H}_{\text{hv}}(R(\mathbf{Z})) \\ &\geq \mathbb{E}_{R(\mathbf{Z}, \mathbf{C})}[\log f(\mathbf{Z}, \mathbf{X})] - \mathbb{E}_{R(\mathbf{Z}, \mathbf{C})}[\log R(\mathbf{Z}, \mathbf{C})] + \mathbb{E}_{R(\mathbf{Z}, \mathbf{C})}[\log S(\mathbf{C}|\mathbf{Z})] \\ &:= \mathcal{L}'(\text{Hierarchical ELBO}). \end{aligned} \quad (15)$$

A derivation of the inequality in line 15. The inequality comes from the decomposition of the entropy  $\mathcal{H}_{\text{hv}}$  of the hierarchical distribution. The proof of the inequality is based on the proof from [53] :

$$\begin{aligned} \mathcal{H}_{\text{hv}}(R(\mathbf{Z})) &= -\mathbb{E}_{R_{\text{hv}}(\mathbf{Z})}[\log R_{\text{hv}}(\mathbf{Z})] \\ &= -\mathbb{E}_{R_{\text{hv}}(\mathbf{Z})}[\log R_{\text{hv}}(\mathbf{Z}) - \mathbf{KL}(R_{\mathbf{C}|\mathbf{Z}}(\mathbf{C}|\mathbf{Z}); R_{\mathbf{C}|\mathbf{Z}}(\mathbf{C}|\mathbf{Z}))] \\ &\geq -\mathbb{E}_{R_{\text{hv}}(\mathbf{Z})}[\log R_{\text{hv}}(\mathbf{Z}) + \mathbf{KL}(R_{\mathbf{C}|\mathbf{Z}}(\mathbf{C}|\mathbf{Z}); S(\mathbf{C}|\mathbf{Z}))] \\ &= -\mathbb{E}_{R_{\text{hv}}}[\mathbb{E}_{R(\mathbf{Z})}[\log R_{\text{hv}}(\mathbf{Z})] + \log R_{\mathbf{C}|\mathbf{Z}}(\mathbf{C}|\mathbf{Z}) - \log S(\mathbf{C}|\mathbf{Z})] \\ &= -\mathbb{E}_{R(\mathbf{Z}, \mathbf{C})}[\log R_{\text{hv}}(\mathbf{Z}) + \log R_{\mathbf{C}|\mathbf{Z}}(\mathbf{C}|\mathbf{Z}) - \log S(\mathbf{C}|\mathbf{Z})] \\ &= -\mathbb{E}_{R(\mathbf{Z}, \mathbf{C})}[\log R_{\mathbf{Z}, \mathbf{C}}(\mathbf{Z}, \mathbf{C}) - \log S(\mathbf{C}|\mathbf{Z})] \end{aligned} \quad (16)$$

□

### A.2 Preservation of $\mathbb{E}_{R(\mathbf{Z}, \mathbf{C})}[\log f(\mathbf{Z})]$

Here we show that the term for  $\mathbb{E}_{R(\mathbf{Z}, \mathbf{C})}[\log f(\mathbf{Z})]$  as written in Eq. (7) is the same as in prior studies such as Daudin et al. [23]

$$\begin{aligned} \mathbb{E}_{R(\mathbf{Z}, \mathbf{C})}[\log f(\mathbf{Z})] &= \sum_i \sum_q \left( P_q \tau_{iq} \log \alpha_q + (1 - P_q) \tau_{iq} \log \alpha_q \right) \\ &= \sum_q (P_q + (1 - P_q)) \left( \sum_i \tau_{iq} \log \alpha_q \right) \\ &= \sum_{i, q} \tau_{iq} \log \alpha_q. \end{aligned}$$

### A.3 Derivation for Expected Log Likelihood

Description of the form of the joint likelihood in Equation (8) in Section 3.4:



**Proposition 2.** *The expected log likelihood of the multivariate normal distribution  $f(\mathbf{Z}, \mathbf{C})$  with respect to  $R(\mathbf{Z}, \mathbf{C})$  is written as*

$$\mathbb{E}_{R(\mathbf{Z}, \mathbf{C})}[\log f(\mathbf{X}, \mathbf{Z})] = \mathbb{E}_{R(\mathbf{Z}, \mathbf{C})}[\log f(\mathbf{X}|\mathbf{Z})] + \sum_i \sum_q \tau_{iq} \log \alpha_q$$

*Proof.*

$$\begin{aligned} \mathbb{E}_{R(\mathbf{Z}, \mathbf{C})}[\log f(\mathbf{X}, \mathbf{Z})] &= \mathbb{E}_{R(\mathbf{Z}, \mathbf{C})}[\log f(\mathbf{X}|\mathbf{Z})] + \mathbb{E}_{R(\mathbf{Z}, \mathbf{C})}[\log f(\mathbf{Z})] \\ &= \mathbb{E}_{R(\mathbf{Z}, \mathbf{C})}[\log f(\mathbf{X}|\mathbf{Z})] + \log \Psi \sum_i \sum_q P_q \tau_{iq} \log \alpha_q \\ &\quad + \log(1 - \Psi) \sum_i \sum_q (1 - P_q) \tau_{iq} \log \alpha_q \\ &= \mathbb{E}_{R(\mathbf{Z}, \mathbf{C})}[\log f(\mathbf{X}|\mathbf{Z})] + \sum_{i,q} \left( P_q \tau_{iq} \log \alpha_q + (1 - P_q) \tau_{iq} \log \alpha_q \right) \\ &= \mathbb{E}_{R(\mathbf{Z}, \mathbf{C})}[\log f(\mathbf{X}|\mathbf{Z})] + \sum_{i,q} \tau_{iq} \log \alpha_q \end{aligned} \tag{17}$$

□

#### A.4 Derivation of Joint Distribution $\mathbb{E}_{R(\mathbf{Z}, \mathbf{C})}[\log R(\mathbf{Z}, \mathbf{C})]$

The expectation of the log of the joint variational distribution is as follows:

$$\begin{aligned} \mathbb{E}_{R(\mathbf{Z}, \mathbf{C})}[\log R(\mathbf{Z}, \mathbf{C})] &= \mathbb{E}_{R(\mathbf{Z}, \mathbf{C})}[\log R(\mathbf{Z}|\mathbf{C})] + \mathbb{E}_{R(\mathbf{Z}, \mathbf{C})}[\log R(\mathbf{C})] \\ &= \sum_i \sum_q \left( (1 - P_q) \mathbb{E} Z_{iq} \log(\tau_{iq}) + P_q \mathbb{E} Z_{iq} \log(\tau_{iq}) \right) + \mathbb{E}[\log R(\mathbf{C})] \\ &= \sum_{i,q} \tau_{iq} \log \tau_{iq} + \sum_q \left( P_q \log P_q + (1 - P_q) \log(1 - P_q) \right) \end{aligned}$$

## B Details for Hierarchical ELBO

This section has the unabridged expressions for the hierarchical ELBO as well as the derivations for these expressions.

### B.1 Log likelihood Part of the ELBO

The log likelihood portion of the ELBO is written as :

$$\begin{aligned} &\mathbb{E}_{R_{\mathbf{X}}}[\log(f(\mathbf{X}|\mathbf{Z}))] \\ &= \sum_q P_q \sum_i \sum_j \tau_{iq} \tau_{jq} \left( \frac{1}{2} (\mathbf{X}_{ij} - \boldsymbol{\mu}_q)^T \boldsymbol{\Sigma}_q^{-1} (\mathbf{X}_{ij} - \boldsymbol{\mu}_q) - (2\pi)^{K/2} (\log |\boldsymbol{\Sigma}_q|)^{1/2} \right) \tag{18} \\ &\quad + \sum_q (1 - P_q) \sum_i \sum_j \tau_{iq} \tau_{jq} \left( \frac{1}{2} (\mathbf{X}_{ij} - \boldsymbol{\mu}_{AN})^T \boldsymbol{\Sigma}_{AN}^{-1} (\mathbf{X}_{ij} - \boldsymbol{\mu}_{AN}) - (2\pi)^{K/2} (\log |\boldsymbol{\Sigma}_{AN}|)^{1/2} \right) \\ &\quad + \sum_q \sum_{l:l \neq q} \sum_i \sum_j \tau_{iq} \tau_{jl} \left( \frac{1}{2} (\mathbf{X}_{ij} - \boldsymbol{\mu}_{AN})^T \boldsymbol{\Sigma}_{AN}^{-1} (\mathbf{X}_{ij} - \boldsymbol{\mu}_{AN}) - (2\pi)^{K/2} (\log |\boldsymbol{\Sigma}_{AN}|)^{1/2} \right). \end{aligned}$$

## B.2 Expression for Hierarchical ELBO

The full form of the ELBO is the log likelihood part plus the membership probabilities, entropy, and their hierarchical counterparts:

$$\begin{aligned}
\mathcal{L}' = & \\
& \sum_q P_q \sum_i \sum_j \tau_{iq} \tau_{jq} \left( \frac{1}{2} (\mathbf{X}_{ij} - \boldsymbol{\mu}_q)^T \boldsymbol{\Sigma}_q^{-1} (\mathbf{X}_{ij} - \boldsymbol{\mu}_q) - (2\pi)^{K/2} (\log |\boldsymbol{\Sigma}_q|)^{1/2} \right) \\
& + \sum_q (1 - P_q) \sum_i \sum_j \tau_{iq} \tau_{jl} \left( \frac{1}{2} (\mathbf{X}_{ij} - \boldsymbol{\mu}_{AN})^T \boldsymbol{\Sigma}_{AN}^{-1} (\mathbf{X}_{ij} - \boldsymbol{\mu}_{AN}) - (2\pi)^{K/2} (\log |\boldsymbol{\Sigma}_{AN}|)^{1/2} \right) \\
& + \sum_q \sum_{l:l \neq q} \sum_i \sum_j \tau_{iq} \tau_{jl} \left( \frac{1}{2} (\mathbf{X}_{ij} - \boldsymbol{\mu}_{AN})^T \boldsymbol{\Sigma}_{AN}^{-1} (\mathbf{X}_{ij} - \boldsymbol{\mu}_{AN}) - (2\pi)^{K/2} (\log |\boldsymbol{\Sigma}_{AN}|)^{1/2} \right) \\
& + \sum_{i,q} \tau_{iq} \log \alpha_q - \sum_q \sum_i \tau_{iq} \log \tau_{iq} - \\
& \sum_q \left( P_q \log P_q + (1 - P_q) \log(1 - P_q) \right) + \sum_i \sum_q \left( P_q \log \Psi + (1 - P_q) \log(1 - \Psi) \right) \tau_{iq}
\end{aligned}$$

This is the full expression for the hierarchical ELBO as described in Section 3.5.

## B.3 Calculation of Hierarchical ELBO

The hierarchical ELBO is written as:

$$\mathcal{L}' = \mathbb{E}_{R(\mathbf{Z}, \mathbf{C})} \log f(\mathbf{X}, \mathbf{Z}) + \mathbb{E}_{R(\mathbf{Z}, \mathbf{C})} [\log R(\mathbf{C}, \mathbf{Z})] + \mathbb{E}_{R(\mathbf{Z}, \mathbf{C})} [\log S(\mathbf{C}|\mathbf{Z})]$$

The joint distributions of  $R(\mathbf{Z}, \mathbf{C})$  and  $S(\mathbf{C}|\mathbf{Z})$  are as follows:

$$\begin{aligned}
R(\mathbf{Z}, \mathbf{C}) &= R(\mathbf{Z}|\mathbf{C})R(\mathbf{C}) \\
&= \prod_q \prod_i \left( \tau_{iq}^{Z_{iq}} \right)^{C_q} \left( \prod_i \tau_{iq}^{Z_{iq}} \right)^{1-C_q} \cdot \prod_q P_q^{C_q} (1 - P_q)^{1-C_q}.
\end{aligned}$$

where  $R(\mathbf{C}) = \prod_q P_q^{C_q} (1 - P_q)^{1-C_q}$ . Moreover, the ‘recursive’ variational approximation for noise memberships  $\mathbf{C}$  given the memberships  $\mathbf{Z}$

$$S(\mathbf{C}|\mathbf{Z}) = \prod_i \prod_q \left( \Psi^{C_q} (1 - \Psi)^{1-C_q} \right)^{Z_{iq}}.$$

The global signal rate  $\Psi := \mathbb{P}(NB)$  (Definition 4) represent the *prior* probabilities of each group membership  $C_q$ . Combined with the conditional distribution of  $\mathbf{C}$  given  $\mathbf{Z}$ , the hierarchical ELBO  $\mathcal{L}'$  is written as

$$\mathcal{L}' = \mathbb{E}_{R(\mathbf{Z}, \mathbf{C})} \log f(\mathbf{X}, \mathbf{Z}) + \mathbb{E}_{R(\mathbf{Z}, \mathbf{C})} [\log R(\mathbf{C}, \mathbf{Z})] + \mathbb{E}_{R(\mathbf{Z}, \mathbf{C})} [\log S(\mathbf{C}|\mathbf{Z})]$$

The first term  $\mathbb{E}_{R(\mathbf{Z}, \mathbf{C})} \log f(\mathbf{X}, \mathbf{Z})$  can be factored out into  $\mathbb{E}_{R(\mathbf{Z}, \mathbf{C})} [\log f(\mathbf{X}|\mathbf{Z}) + \log f(\mathbf{Z})]$  and then be written as :

$$\mathbb{E}_{R(\mathbf{Z}, \mathbf{C})} [\log f(\mathbf{X}, \mathbf{Z})] = \mathbb{E}_{R(\mathbf{Z}, \mathbf{C})} [\log f(\mathbf{X}|\mathbf{Z})] + \sum_{i,q} \tau_{iq} \log \alpha_q$$

where  $f(\cdot)$  as the multivariate normal frequency described in Eq. (18) in Appendix B.

and that the second joint mean-field distribution term can be similarly factorized into  $\mathbb{E}_{R(\mathbf{Z}, \mathbf{C})}[\log R(\mathbf{C}|\mathbf{Z}) + \log R(\mathbf{Z})]$ . The second term is written as:

$$\mathbb{E}_{R(\mathbf{Z}, \mathbf{C})}[\log R(\mathbf{Z}, \mathbf{C})] = \sum_i \sum_q \tau_{iq} \log \tau_{iq} + \sum_q \left( P_q \log P_q + (1 - P_q) \log(1 - P_q) \right).$$

The derivation of this term can be found in Appendix A.4. Finally, the expectation of the third term  $S(\mathbf{C}|\mathbf{Z})$ , described by Ranganath et al. as the ‘recursive variational approximation’ [53] for  $R(\cdot)$ , is directly derived from the earlier expression  $S(\mathbf{C}|\mathbf{Z})$  can be written as

$$\mathbb{E}_{R(\mathbf{Z}, \mathbf{C})} \log S(\mathbf{C}|\mathbf{Z}) = \sum_i \sum_q \left( P_q \log \Psi + (1 - P_q) \log(1 - \Psi) \right) \tau_{iq}.$$

## C Calculations for VEM Algorithm

This section gives derivations for every step of the Variational EM algorithm in Section 4.

### C.1 Optimizing Membership Probabilities $\tau$ in E-Step

We find optimal values for each  $\tau_{iq}$  by solving this following equation, which is described in Section 4.1.1:

$$\begin{aligned} \frac{\partial}{\partial \tau_{iq}} \mathcal{L} &= \log(\alpha_q) + \sum_{k=1, \dots, K} \sum_{j=1, \dots, n} \tau_{jl} \left( P_q f(X_{ij}^k, \boldsymbol{\mu}_q, \boldsymbol{\Sigma}_q) + (1 - P_q) f(X_{ij}^k, \boldsymbol{\mu}_{AN}, \boldsymbol{\Sigma}_{AN}) \right. \\ &\quad \left. + \sum_{l \leq Q: l \neq q} f(X_{ij}^k, \boldsymbol{\mu}_{AN}, \boldsymbol{\Sigma}_{AN}) \right) - \log(\tau_{iq}) - 1 + P_q \log \Psi + (1 - P_q) \log(1 - \Psi) \\ &:= 0, \end{aligned}$$

rearranging  $\tau_{iq}$  we solve this equation using a fixed point iteration procedure

### C.2 Estimation of Noise Probability $P_q$ in E-Step

We posit that variational variables  $P_q$  that serve as the ‘soft’ versions of  $C_q$  can be approximated by estimating the probability of block  $q$  being a ‘signal’ block or noise block. The terms  $\mathbb{E}_{R(\mathbf{Z}, \mathbf{C})} \log f(\mathbf{X}|\mathbf{Z})$ ,  $\mathbb{E}[\log R(\mathbf{C})]$ ,  $\mathbb{E}[\log S(\mathbf{C}|\mathbf{Z})]$  in  $\mathcal{L}'$  are dependent on  $\mathbf{C}$ . Practically, because we need to normalize for  $N_q$ , which is  $1 - P_q$ , that variable is more simple (if not the only possible tractable option).

$$\begin{aligned} \frac{\partial}{\partial N_q} \mathcal{L}' &= \frac{\partial}{\partial N_q} \mathbb{E}_{R(\mathbf{Z}, \mathbf{C})}[\log f(\mathbf{X}|\mathbf{Z})] - \log N_q + \log(1 - N_q) - (\log \Psi + \log(1 - \Psi)) \sum_i \tau_{iq} \\ &:= 0 \end{aligned}$$

where the first term is  $f(\cdot)$  is the portion of the multivariate normal density as described in Equation (18).

$$\sum_k \sum_{i,j} \tau_{iq} \tau_{jq} \left( f(X_{ij}^k, \boldsymbol{\mu}_q, \boldsymbol{\Sigma}_q) - f(X_{ij}^k, \boldsymbol{\mu}_{AN}, \boldsymbol{\Sigma}_{AN}) + \log \left( \frac{1 - \Psi}{\Psi} \right) \right) = \log \left( \frac{N_q}{1 - N_q} \right)$$

So then, after rearranging:

$$\widehat{N}_q = \left( 1 + \left[ \exp \left( \sum_k \sum_i \sum_j \tau_{iq} \tau_{jq} \left( f(X_{ij}^k, \boldsymbol{\mu}_q, \boldsymbol{\Sigma}_q) - f(X_{ij}^k, \boldsymbol{\mu}_{AN}, \boldsymbol{\Sigma}_{AN}) \right) + \log \left( \frac{1 - \Psi}{\Psi} \right) \right) \right] \right)^{-1}. \quad (19)$$

Then the final  $N_q$  estimates are made after normalizing all  $\widehat{N}_q$  such that they sum to one. Finally, the  $P_q$  estimates are made by subtracting  $N_q$  from 1.

### C.3 Derivation of Signal Terms for M-Step

The closed-form estimate of the parameter for the mean vector  $\boldsymbol{\mu}_q$  for each block  $q$  from the M-step is

$$\begin{aligned} \widehat{\boldsymbol{\mu}}_q &= \frac{\sum_{i,j} \tau_{iq} \tau_{jq} \mathbf{X}_{ij}}{\sum_{i,j} \tau_{iq} \tau_{jq}} P_q + \frac{\sum_{i,j} \tau_{iq} \tau_{jq} \boldsymbol{\mu}_{AN}}{\sum_{i,j} \tau_{iq} \tau_{jq}} \cdot (1 - P_q) \\ &= \frac{\sum_{i,j} \tau_{iq} \tau_{jq} \mathbf{X}_{ij}}{\sum_{i,j} \tau_{iq} \tau_{jq}} P_q + \boldsymbol{\mu}_{AN} (1 - P_q) \end{aligned}$$

Assuming convergence of  $P_q$  to either 0 or 1 within the context of the variational iterations, the theoretical value of

$$\boldsymbol{\mu}_q = \begin{cases} \frac{\sum_{i,j} \tau_{iq} \tau_{jq} \mathbf{X}_{ij}}{\sum_{i,j} \tau_{iq} \tau_{jq}} & \text{if } q \text{ is Signal: } P_q = 1 \\ \boldsymbol{\mu}_{AN} & \text{if } q \text{ is Noise: } P_q = 0 \end{cases}$$

Similarly to mean calculations, the variance calculations (along diagonals) are :

$$\begin{aligned} \widehat{\boldsymbol{\Sigma}}_q &= \frac{\sum_{i,j} \tau_{iq} \tau_{jq} (\mathbf{X}_{ij} - \boldsymbol{\mu}_q)^2}{\sum_{i,j} \tau_{iq} \tau_{jq}} \cdot P_q + \boldsymbol{\Sigma}_{AN} \cdot (1 - P_q) \\ &= \begin{cases} \sum_{i,j} \tau_{iq} \tau_{jq} (\mathbf{X}_{ij} - \boldsymbol{\mu}_q)^2 / \sum_{i,j} \tau_{iq} \tau_{jq} & \text{if } q \text{ is Signal: } P_q = 1 \\ \boldsymbol{\Sigma}_{AN} & \text{if } q \text{ is Noise: } P_q = 0 \end{cases} \end{aligned}$$

The cross-term for two layers  $h, k$  is written as:

$$\begin{aligned} \widehat{\boldsymbol{\Sigma}}_{hk,q} &= \frac{\sum_{i,j} \tau_{iq} \tau_{jq} (\mathbf{X}_{k,ij} - \boldsymbol{\mu}_{q,k})(\mathbf{X}_{ij}^h - \boldsymbol{\mu}_{q,h})}{\sum_{i,j} \tau_{iq} \tau_{jq}} \cdot P_q + 0 \cdot (1 - P_q) \\ &= \frac{\sum_{i,j} \tau_{iq} \tau_{jq} (\mathbf{X}_{ij}^k - \boldsymbol{\mu}_{q,k})(\mathbf{X}_{ij}^h - \boldsymbol{\mu}_{q,h})}{\sum_{i,j} \tau_{iq} \tau_{jq}} \cdot P_q \end{aligned}$$

The element-wise correlations at iteration  $t$  across layers  $h, k$  ( $h \neq k$ ) are then calculated as

$$\hat{\rho}_q^{h,k} = \frac{\widehat{\Sigma}_{hk}^q}{\sqrt{\widehat{\Sigma}_q^h \widehat{\Sigma}_q^k}}.$$

Finally, the putative correlation (across all layers) for block  $q$  can be calculated as

$$\hat{\rho}_q = \max_{h,k} \hat{\rho}_q^{h,k}.$$

#### C.4 Derivation for $\boldsymbol{\mu}_{AN}$ and $\boldsymbol{\Sigma}_{AN}$

This is derivation for (4.2.1) To calculate the global parameters, the global noise probability term  $\Psi$  defined previously is

$$\begin{aligned} \widehat{\boldsymbol{\mu}}_{AN} &= \mathbb{E}_{R_{\mathbf{X}}(\mathbf{Z}, \mathbf{C})}[\boldsymbol{\mu}_{AN}] \\ &= \mathbb{P}(B_q \text{ not } NB) \mathbb{E}_{R(\mathbf{Z}, \mathbf{C})}[\boldsymbol{\mu}_{AN} | B_q \text{ not } NB] \\ &\quad + \mathbb{P}(B_q = NB) \mathbb{E}_{R(\mathbf{Z}, \mathbf{C})}[\boldsymbol{\mu}_{AN} | \{B_q = NB\}]; \quad q : 1 \leq q \leq Q \\ &= \Psi \frac{\sum_{j,i} \sum_{l,q:q \neq l} \tau_{iq} \tau_{jl} \mathbf{X}_{ij}}{\sum_{j,i} \sum_{l,q:q \neq l} \tau_{iq} \tau_{jl}} + (1 - \Psi) \frac{\sum_{j,i} \sum_q \tau_{iq} \tau_{jq} (1 - P_q) \mathbf{X}_{ij}}{\sum_{j,i} \sum_q \tau_{iq} \tau_{jq} (1 - P_q)}, \end{aligned}$$

$\widehat{\boldsymbol{\Sigma}}_{AN}$  can also be calculated in a similar way.

#### C.5 Derivation of $\Psi$

Derivation of  $\Psi$  that was first defined in Definition 4. Let  $\{NB\}$  represent the event that there exists a Noise Block in the multilayer graph system. Then we write the indicator for this event as  $\mathbf{1}(NB)$  with probability  $\mathbb{P}(NB)$ .

$$\begin{aligned} \Psi &= \mathbb{P}(B_q \neq NB; \forall q : 1 \leq q \leq Q) \\ &= \mathbb{P}(C_q = 1; \forall q : 1 \leq q \leq Q) \\ &= 1 - \mathbb{P}(\text{Global average rate of } q \text{ s.t. } C_q = 0; \forall q : 1 \leq q \leq Q) \\ &= 1 - 1/Q \\ &= (Q - 1)/Q \end{aligned}$$

## D Details on Stochastic Variational Inference

To apply stochastic variational inference, we first define the time-variable step size  $\delta_t$  to retain some memory from previous iteration. A time-varying  $\delta_t \in (0, 1)$  is selected to satisfy the convexity assumption of (1)  $\sum_t \delta_t = \infty$  and (2)  $\sum_t \delta_t^2 < \infty$  as outlined in [31], for some  $\kappa \in (.5, 1)$

$$\delta_t = (t + 1)^{-\kappa}.$$

However, this criteria needs to be changed when the stochastically sampled variables represent memberships. Empirically, the samples converge at a fast rate when the initial

“burn in” steps are subsampled, with subsample sizes increasing with each successive step. A potentially major impediment, if subsampling does not take place, may arise from the slow computation speed in early steps where initialized estimates are not near the optimal values. As such, the step sizes are set as such:

$$\delta_t = \min \left( a + \left( \frac{t}{t+1} \right)^\kappa n, n \right).$$

$a$  and  $\kappa$  are constants.  $a$  governs the smallest subsample size and  $\kappa > 1$  governs the rate of increase for subsample size at each step size, with the maximum possible subsample size  $n$ . A larger  $a$  means a larger starting subsample, and a larger  $\kappa$  means a faster rate of increase in subsample size.

Empirically, for a wide range of simulations, an effective choice for  $a$  is between 100 to 200 (depending on network size) and for  $\kappa$  is 2. These values are chosen to ensure computational efficiency in addition to accuracy: computation times for initial values are much slower if the parameter estimates are far from the optimal values which maximize the ELBO, so smaller sample sizes in earlier iterations will economize computation by producing more local minima, while later iterations will yield more globally accurate estimates [31].

## E Identifiability and Connection to Prior Models

In the introduction, we bring up the *Affiliation model* in Section 1.2 as an example of prior work describing global noise on networks. On a single weighted network, a simple parametric model known as the affiliation model described in Allman et al. [4] is formulated as follows with piecewise global fixed rates both for probability and rate for

$$\mu_{ql} = (1 - p_{ql})\delta_0 + p_{ql}F_{ql}(\theta_{\text{in}}\mathbf{1}_{q=l} + \theta_{\text{out}}\mathbf{1}_{q \neq l}); \quad 1 \leq q, l \leq Q$$

where probability  $p_{ql}$  is the sparsity parameter, continuous distribution  $F_{ql}(\theta_{ql})$  with parameter  $\theta_{ql}$  and  $\delta_0$  is a dirac mass at zero, and with probability

$$p_{ql} = \alpha\mathbf{1}_{q=l} + \beta\mathbf{1}_{q \neq l}; \quad .$$

One can conceive of the weighted stochastic blockmodel as a special case of the *general form of mixture models for random graphs* described in [4]. For graph  $X$  where each weighted edge is  $X_{ij}$  between nodes  $i, j$ :

$$\forall q, l \in \{1, \dots, Q\} \quad X_{ij} | \{Z_{iq}Z_{jl} = 1\} \sim p_{ql}f(\cdot, \theta_{ql}) + (1 - p_{ql})\delta_0(\cdot),$$

where  $p_{ql}$  serves as the sparsity parameter between 0 and 1, which represents the proportion of .  $f(\cdot, \theta_{ql})$  represents the parametric family of distributions at specified in group-interactions  $q$  and  $l$ . The conditional distribution of  $X_{ij}$  is a mixture of the Dirac distribution at zero representing non-present edges. The proposed SBANM model can also be viewed as an instance of the generalized model above. Methodologically, it is a mixture of the affiliation model and the weighted multilayer SBM. Matias et al. [44] discuss identifiability of block parameters in multilayer SBMs. The authors cite [4] in setting the conditions for identifiability for weighted SBMs over multiple layers. Since the affiliation model is also proven to be identifiable [3], we posit that SBANM should also be identifiable, but leave more detailed justifications in future work.

## F Parsimony Compared to Other Models

SBANM is a parsimonious compared to most other models. If inter-block interactions ( $B_q \neq B_l$ ) are all unique, as in some models [43, 44] then this leads to overparametrization, especially at high dimensions ( $\approx K \times \frac{Q(Q-1)}{2}$  parameters). The number of parameters may be reasonable for binary and Poisson-distributed multilayer networks, but will quickly inflate in the multivariate Gaussian case. SBANM yields  $3KQ + 2K$  parameters comprising the  $2KQ$  mean and (diagonal elements of) variance parameters  $\{(\boldsymbol{\mu}_q, \boldsymbol{\Sigma}_q)\}_{q:1 \leq q \leq Q}$ ,  $KQ$  correlation parameters  $\{\rho_q\}_{q:1 \leq q \leq Q}$ , and  $2K$  noise parameters  $(\boldsymbol{\mu}_{AN}, \boldsymbol{\Sigma}_{AN})$ . As  $Q$  becomes large, the number of parameters increases quadratically in the canonical weighted SBM but linearly in SBANM. As  $K$  becomes large, also, the rate of increase for parameters in the proposed method is smaller than that in existing methods. This advantage is demonstrated in computing time comparisons in Section 5.1.5.

## G Parameter Recovery of Simulations

Estimates of parameters are reasonably retrieved from the SBANM algorithm. There does not seem to be much systemic bias in the estimates as empirical means of differences between estimated and true parameters are centered around 0. Median percentage differences, across all estimated parameters, between the estimates and true values are between 20 to 25% for bivariate, and 10-20% for trivariate networks. Histograms for the mean and variance parameters (each distinct parameter is treated like an observation) show essentially matching distributions between estimates and ground truth parameters for means (5).

A slight discrepancy between distributions for variance parameters ( $\sigma_{q,k}^2$  for  $k = 1, 2, 3$ ) among trivariate networks. This slight bias may be related again to the curse of dimensionality and, while does not seem to elicit too severe a problem in the clustering results, may be investigated in future endeavors.

Percentage differences between the estimated and ground-truth parameters also show moderately accurate recovery in both bivariate and trivariate networks. The lowest 25% quartiles for all parameters are between 0 and 3 percent and show that these estimates are very close to the ground truths. Conflated with the relatively higher mean and median differences, the low 1st quartiles show that accuracy for parameter runs seem to occur along a binary: either estimates are very close to their targets, or they are fairly far off. Some of the high percentage differences may arise from small ground-truth values, which are divided to calculate percentage differences. Others may arise from the mismatches in clustering memberships (in the trivariate case, as there is a near-perfect recovery rate for the bivariate simulations).

Finally, we describe the large-network simulations. Single instances of networks with  $n = 1000$  and  $2000$  are generated for  $Q = 4$  and  $5$ . Results yielded exact recovery for memberships and within 5% errors for parameters.

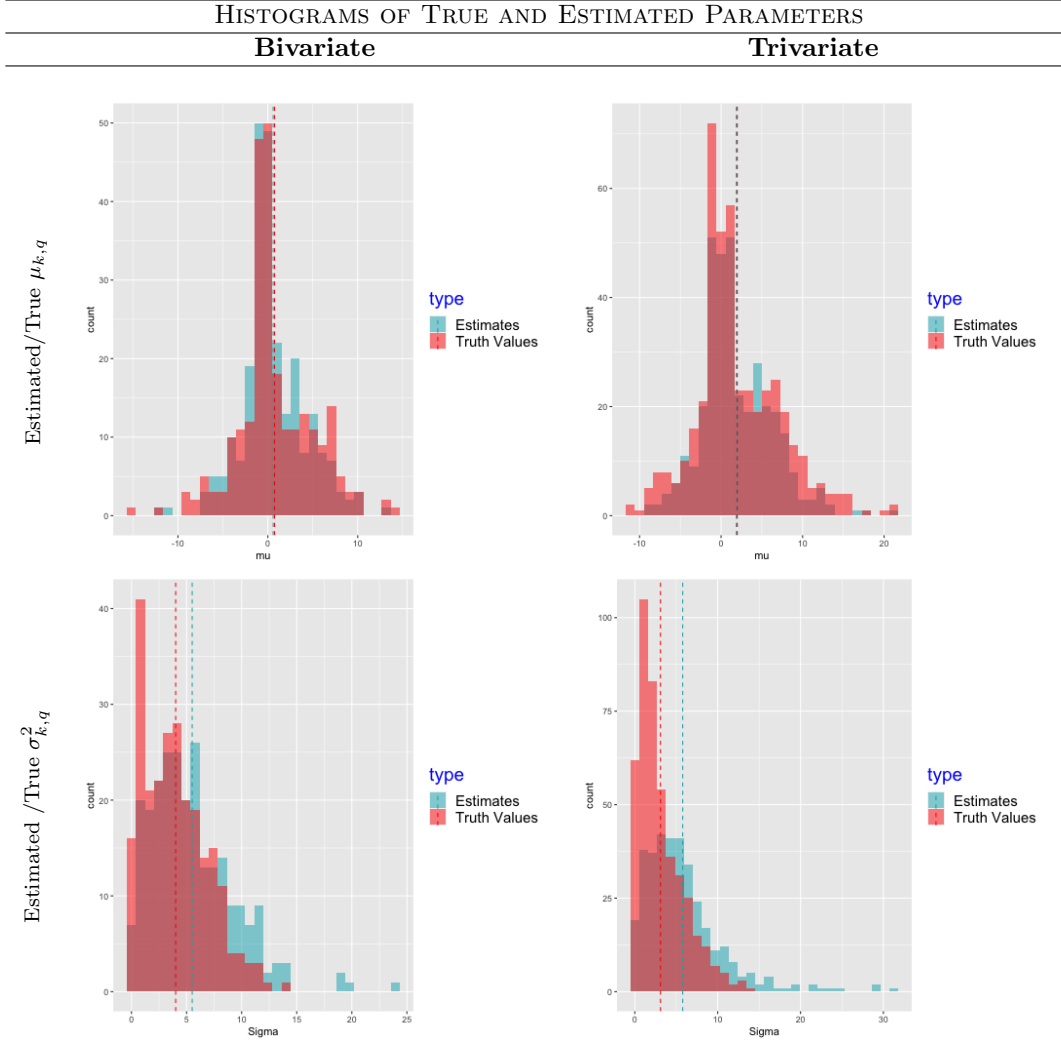


Figure 5: Histograms of ground truth (red) and estimate (blue) parameter values for the 2-layer and 3-layer networks compared to the estimated parameters from the algorithm. Parameters across layers are all plotted together. Dashed lines demarcate the empirical means of these estimated and ground truth parameters. For ground truths (red), these empirical means are .75 for  $\mu_{k,q}$  (bivariate, top left), 1.98 for  $\mu_{k,q}$  (trivariate, top right), 4.01 for  $\sigma_{k,q}^2$  (bivariate, bottom left), 3.10 for  $\sigma_{k,q}^2$  (trivariate, bottom right). For estimates of parameters, they are .58 for  $\mu_{k,q}$  (bivariate, top left), 1.84 for  $\mu_{k,q}$  (trivariate, top right), 5.51 for  $\sigma_{k,q}^2$  (bivariate, bottom left), 5.58 for  $\sigma_{k,q}^2$  (trivariate, bottom right).



## H Demographic Characteristics of PNC Results

Block	$n$	Age	Env	%AA	%L	%F
<b>MP: 4 Gps</b>						
● $N$	247	15	-1	33	6	55
● $S_1$	2552	14	14	27	5	49
● $S_2$	852	15	-14	41	6	51
● $S_3$	1485	15	-2	34	7	57
<b>MP: 3 Gps</b>						
● $N$	408	15	-17	41	6	45
● $S_1$	2552	14	14	27	5	49
● $S_2$	2176	15	-4	35	7	57
<b>AP: 5 Gps</b>						
● $N$	128	19	-10	35	7	53
● $S_1$	2	19	54	0	0	50
● $S_2$	338	19	-21	39	7	59
● $S_3$	792	19	-3	34	6	59
● $S_4$	603	19	-9	37	8	61
<b>AP: 4 Gps</b>						
● $N$	48	19	-28	38	10	52
● $S_1$	1495	19	-6	35	7	59
● $S_2$	39	19	-41	46	8	56
● $S_3$	281	20	-13	37	5	65

Table 5: Demographic characteristics for the runs. The columns represent respectively: age, environmental factors (Z-scores multiplied by 100), % African American, % Latinx, and % female